AGU PUBLICATIONS

Water Resources Research

RESEARCH ARTICLE
10.1002/2017WR020554

Key Points:
- A fully analytical model accounting for the nonstationarity of the unsaturated flow variables as influenced by the water table is presented
- Simple (closed form) expressions for the second-order moments of the flow variables and the mean head are derived
- The good agreement between predictions and real data confirmed the scientific consistency of the developed model

Supporting Information:
- Supporting Information S1
- Data Set S1

Correspondence to:
G. Severino,
gerardo.severino@unina.it

Citation:
Severino, G., M. Scarfato, and A. Comegna (2017), Stochastic analysis of unsaturated steady flows above the water table, *Water Resour. Res.*, *53*, 6687–6708, doi:10.1002/2017WR020554.

Received 7 FEB 2017
Accepted 8 JUL 2017
Accepted article online 19 JUL 2017
Published online 8 AUG 2017

Stochastic analysis of unsaturated steady flows above the water table

Gerardo Severino[1], Maddalena Scarfato[1], and Alessandro Comegna[2]

[1]Department of Agricultural Sciences, Division of Water Resources Management and Biosystems Engineering, University of Naples-Federico II, Naples, Italy, [2]School of Agricultural Forestry Food and Environmental Sciences, University of Basilicata, Italy

Abstract Steady flow takes place into a three-dimensional partially saturated porous medium where, due to their spatial variability, the saturated conductivity K_s, and the relative conductivity K_r are modeled as *random space functions* (RSF)s. As a consequence, the *flow variables* (FVs), i.e., pressure-head and specific flux, are also RSFs. The focus of the present paper consists into quantifying the uncertainty of the FVs above the water table. The simple expressions (most of which in closed form) of the second-order moments pertaining to the FVs allow one to follow the transitional behavior from the zone close to the water table (where the FVs are nonstationary), till to their far-field limit (where the FVs become stationary RSFs). In particular, it is shown how the stationary limits (and the distance from the water table at which stationarity is attained) depend upon the statistical structure of the RSFs K_s, K_r, and the infiltrating rate. The mean pressure head $\langle\Psi\rangle$ has been also computed, and it is expressed as $\langle\Psi\rangle=\Psi_0(1+\psi)$, being ψ a characteristic heterogeneity function which modifies the zero-order approximation Ψ_0 of the pressure head (valid for a vadose zone of uniform soil properties) to account for the spatial variability of K_s and K_r. Two asymptotic limits, i.e., close (near field) and away (far field) from the water table, are derived into a very general manner, whereas the transitional behavior of ψ between the near/far field can be determined after specifying the shape of the various input soil properties. Besides the theoretical interest, results of the present paper are useful for practical purposes, as well. Indeed, the model is tested against to real data, and in particular it is shown how it is possible for the specific case study to grasp the behavior of the FVs within an environment (i.e., the vadose zone close to the water table) which is generally very difficult to access by direct inspection.

1. Introduction

Soil hydraulic properties, such as saturated conductivity, water retention, and relative conductivity have been largely considered as well-defined properties of the unsaturated porous formations [see, e.g., *Hillel*, 1998]. However, in the majority of the hydrological applications, unsaturated flows take place in a complex environment (often termed as *vadose zone*) whose setup changes erratically, thus undermining any attempt to characterize within a deterministic framework the flow (and transport) properties. Such a setup shows discrete and/or continuous variations over several scales, thus making hydraulic properties to do likewise. On the other side, owing to several logistic and economic limitations, hydraulic properties can be measured only at a limited number of positions where their values depend upon the size of the sample(s) as well as the procedure of measurement. Inferring parameters at points where measurements are not available entails a random error [*Sinsbeck and Tartakovsky*, 2015]. In addition to this, measured values are biased by experimental errors. As matter of fact, these errors and uncertainties render the hydraulic parameters RSFs, and the corresponding flow-equations stochastic.

It is a common tenet that an appropriate tool to deal with this uncertainty is the geostatistical approach [*Rubin*, 2003]. Thus, measurements of the hydraulic parameters are regarded as samples of random fields, which in turn are characterized by a multivariate probability density function (or alternatively by ensemble moments). If the statistical properties of the hydraulic parameters can be inferred from measurements, the stochastic flow-equations can be solved either analytically [e.g., *Severino and Indelman*, 2004; *Severino et al*., 2006, 2012a] or numerically [e.g., *Severino and Bartolo*, 2015] by *Monte Carlo simulations* (MCs), and results analyzed in a statistical sense [*Severino et al*., 2007]. MCs are conceptually simple, and they have the advantage to be applicable to a large variety of configurations [see, e.g., *Barajas-Solano and Tartakovsky*, 2016]. However, MCs pose a number of serious drawbacks and

limitations. Indeed, to account for high-frequency fluctuations of the input RSFs, very fine numerical grids are required. As a consequence, each realization (sampling) may result computer-demanding, especially when one deals with three-dimensional flows. In addition, even if MCs converge after a sufficiently large number of runs, there is not a systematic procedure to ascertain whether to consider conclusive (and therefore completed) the MCs (a deep discussion upon these issues can be found in *Jankovic et al*. [2003]; *Russo et al*. [2009]).

To avoid the lack of accuracies attached to the MCs, analytical approaches have been also developed [see, e.g., *Severino*, 2011a, and references therein]. Unlike MCs, analytical methods enable one: (i) to compute the fluctuations of the FVs, and subsequently to obtain (by ensemble averaging) the various (cross)covariances, or (ii) to end up with deterministic equations which are solved for the (cross)covariances. This second avenue (which will be adopted in the present study) is also known as the *method of moments' equation* (MME). The applicability of analytical methods generally relies upon some assumptions, the most relevant of which are: (i) unbounded flow-domain, and (ii) gravity-dominated mean flow [see, e.g., *Yeh et al*., 1985; *Russo*, 1993; *Severino and Santini*, 2005; *Severino et al*., 2009]. In particular, the latter assumption implies that the mean pressure-head is constant within the flow-domain. However, assuming that gravity is the only driving force for the mean flow is sometimes too limiting, especially when one is interested in the flow's behavior close to the water table where, as it is well known, the mean pressure-head is not constant. This renders the problem more difficult, and it is not surprising that very few analytical studies have been carried out toward such a direction. From the stand point of the applications, solving the unsaturated flow in the vicinity of the groundwater is even more important. In fact, in the majority of the cases the water table is located at depths which are completely unaccessible, therefore rendering direct inspection impossible (or extremely time-consuming and expensive). Within such a picture, the use of a reliable model connecting information that can be easily acquired at the soil surface to those at the very deep (difficult to access) locations becomes of paramount relevance.

One of the first attempt to account for the impact of the water table upon the FVs' behavior is from *Andersson and Shapiro* [1983] who analyzed the spatial distribution of the water content in a one-dimensional domain by means of both analytical methods (small perturbations) and MCs. They found that the distance from the water table to the region of "stationarity" depends upon the soil properties as well as the flux at the soil surface. However, in the study of *Andersson and Shapiro* [1983] only the saturated hydraulic conductivity K_s was regarded as a RSF. The pressure-head behavior under the same conditions of the previous study was analyzed by *Indelman et al*. [1993] who adopted the model of *Gardner* [1958] for the relative conductivity K_r. In the region of nonstationarity, the variance of the pressure-head was found sensitive to both the mean flow conditions and to the spatial variability of the soil hydraulic properties. *Tartakovsky et al*. [1999] developed an alternative methodology based upon the Kirchhoff's transformation which enables one to avoid (or delay) any approximation procedure. In order to fully take advantage of the Kirchhoff transformation, *Tartakovsky et al*. [1999] regarded the α-parameter as a random constant. Then, by dealing with a one-dimensional domain and vertical flow conditions, *Tartakovsky et al*. [1999] derived analytical solutions for the covariance and the second-order correction to the pressure-head. A similar analysis in a three-dimensional formation, relying upon MCs, has been conducted by *Russo and Fiori* [2008], who showed that when the water table is located at a sufficiently large depth from the soil surface, one can delineate a region where flow is essentially gravity-dominated (and concurrently the FVs are stationary).

In the present paper, we solve unsaturated steady flow in three-dimensional bounded heterogeneous formations by means of analytical tools, and we aim at computing second-order moments of the FVs. More precisely, we employ a general perturbation procedure to achieve simple (closed-form) results relating into a straightforward manner the statistical structure of the input soil properties to the spatial distribution of the FVs in the vicinity of the water table. The paper is organized as follows: we begin by formulating the mathematical problem in the context of a stochastic framework (section 2), and derive second-order moments for the FVs (sections 3–4). The model is calibrated against to a recently conducted flow experiment in the vadose zone (section 5), and subsequently it is used to grasp the behavior of the FVs in the close vicinity of the water table (section 6). We end up with concluding remarks (section 7).

2. Mathematical Statement of the Problem

Unsaturated steady flow takes place in a three-dimensional domain Ω which is horizontally unbounded, and vertically delimited by the position of the water table ($z = 0$) and the soil surface ($z = L$), i.e.,

$$\Omega=\{\boldsymbol{x} \equiv (x,y,z) : (x,y) \equiv \boldsymbol{x}_h \in \mathbb{R}^2, \quad 0 \le z \le L\} \tag{1}$$

(Figure 1). The governing equations are: (i) the Buckingham-Darcy (constitutive) law, and (ii) the mass-balance law

$$\mathbf{q}(\boldsymbol{x})=-K(\Psi)\nabla(z+\Psi), \qquad \nabla \cdot \mathbf{q}(\boldsymbol{x})=0, \tag{2}$$

respectively. In equation (2), $\mathbf{q} \equiv (q_x, q_y, q_z)^\top$ is the specific flux, $\Psi \equiv \Psi(\boldsymbol{x})$ is the pressure-head, and $K \equiv K(\Psi)$ is the pressure-dependent hydraulic conductivity. Boundary conditions are determined by physical processes at the soil surface and water table. Thus, let q_0 denote a prescribed (negative for infiltration) vertical flux at the soil surface ($z = L$) (as determined either by the rainfall or by the irrigation). This gives rise to a boundary condition:

$$K(\Psi)\left(1+\frac{\partial}{\partial z}\Psi\right)|_{z=L}=-\mathbf{q}\cdot\boldsymbol{e}_z=-q_0\,, \tag{3}$$

being $\boldsymbol{e}_z \equiv (0,0,1)$ the vertical unit pointing outward vector (Figure 1). Generally, flows occurring in the uppermost soil are largely transient as consequence of the high variability of the atmospheric conditions. However, in the close vicinity of the water table the dependence of flow with time results of negligible impact [*Wang et al.*, 2009]. More precisely, *Russo and Fiori* [2008] have demonstrated that, when the water table is deep, the vadose zone can be conceptually decomposed into two distinct zones: a highly transient near-surface zone, and a deeper one where practically steady state flow conditions occur. Within such a zone, an equivalent constant flux q_0 (obtained by averaging the cumulative flux of the net applied water over the relevant time period) provides a good approximation of the cumulative water flux arriving to the water table.

Although the pressure head may fluctuate in the zone close to the water table, the numerical analysis of *Russo and Fiori* [2008] demonstrates that, when the water table is located at sufficiently large depth from the soil surface, a steady spatially uniform head is worth to reconstruct not only the flow regime but also the mass arrivals at the groundwater. Such an approximation applies to very general vadose zones (i.e., of largely different textures) in the presence or absence of vegetation (see discussion in *Russo and Fiori* [2009]). Thus, we assume that the water table ($z = 0$) is at rest, and it separates the unsaturated zone ($\Psi < 0$) from the phreatic one ($\Psi > 0$). Before proceeding further, it is worth also clarifying why, for the present study, the capillary fringe can be neglected. Thus, its thickness is significant when the water table: (i) largely fluctuates in the time [*Li and Yeh*, 1998], and (ii) when the water table is shallow [*Gillham*, 1984]. In addition, such fluctuations are particularly relevant in the coarser soils, and in this case they significantly affect the flow and transport regimes [*Russo and Fiori*, 2009]. However, under steady state conditions (which apply in the present study), the situation is completely reversed, since in the structureless sandy soils (like the one considered in the sequel), the water's raise due to the capillarity-mechanism is highly contrasted by the macropores [e.g., *Zhang and Winter*, 1998; *Zhang*, 2002]. Hence, a boundary condition at the water table reads as:

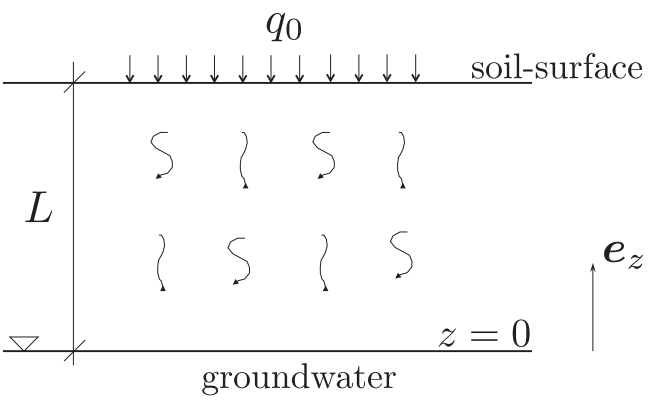

Figure 1. Sketch of a flow taking place into a vadose zone delimitated at the bottom ($z = 0$) by the water table and at the top ($z = L$) by the soil surface.

$$\Psi(\boldsymbol{x})|_{z=0}=0. \tag{4}$$

In order to solve the system of the two equation (2), a functional dependence for $K \equiv K(\Psi)$ must be specified. Several models for K are available in the literature [e.g., *Brooks and Corey*, 1964; *Mualem*, 1976; *Van Genuchten*, 1980]. In the context of the present study, we shall adopt the exponential model of *Gardner* [1958]:

$$K(\Psi) \equiv K_s K_r(\Psi), \qquad K_r(\Psi) = \exp(\alpha \Psi), \tag{5}$$

where K_s and α are the saturation conductivity and a pore-size distribution parameter, respectively. Generally, other conductivity curves have been proved to better reproduce the hydrological soil behavior. However, such curves require a very detailed characterization which is typically carried out at laboratory scale [*Romano et al*., 2011]. Instead, at formation (and even larger) scales the uncertainty of the soil hydraulic properties and the limitations of the in situ sampling devices do not allow gaining a very detailed resolution of the conductivity curve. Thus, owing to these limitations (and wishing to reduce the computational burden), we have adopted [similarly to *Indelman et al*., 1993; *Tartakovsky et al*., 1999, 2004; *Severino and Tartakovsky*, 2015] the *Gardner*'s model. Last, the main difference between the *Gardner*'s and any other model is at the saturation, i.e., $\Psi \sim 0$. Instead, for $\Psi < 0$ (which in the vadose zone is the rule rather than the exception) the hydraulic response of the *Gardner*'s model does not significantly differ from that of any other ones [see, e.g., *Comegna et al*., 1996; *Tartakovsky et al*., 2003].

Due to their erratic variations [see, e.g., *White and Sully*, 1992; *Russo and Bouton*, 1992; *Severino et al*., 2003, 2010; *Fallico et al*., 2016; *Severino et al*., 2016a], the log-transformed parameters $\zeta = \ln \alpha$ and $Y = \ln K_s$ are modeled as *stationary* RSFs. As a consequence, their geometric means: $\alpha_G = \exp\langle\zeta\rangle$ and $K_G = \exp\langle Y\rangle$ are constant with zero-mean fluctuations, i.e., $\langle\zeta'\rangle = \zeta - \langle\zeta\rangle = 0$ and $\langle Y'\rangle = Y - \langle Y\rangle = 0$. Since the conductivity curve (5) depends upon the two RSFs K_s and α, the cross covariance $C_{Y\zeta}$ has to be provided, as well. In line with field-data [see e.g., *Rubin*, 2003], we assume that covariances of the RSFs have axisymmetric structure, i.e.,

$$C_\gamma(x_h, z) = \sigma_\gamma^2 \, \rho_h\left(\frac{x_h}{I_\gamma}\right) \rho_v\left(\frac{z}{\lambda_\gamma I_\gamma}\right) \qquad \gamma = Y, Y\zeta, \zeta \tag{6}$$

being I_γ and λ_γ the horizontal integral scale and the anisotropy-ratio, respectively. The asymmetric (spatial) structure (6) is rather general feature accounting for the typical statistical anisotropies of a vadose zone (a wide survey can be found in *Rubin* [2003]). We adopt α_G^{-1} and K_G as scales for the length and the flux, respectively. As a consequence, equation (2) write as (for simplicity we retain the same notations):

$$\begin{cases} \mathbf{q}(\boldsymbol{x}) = -\exp(Y')\exp[\Psi\exp(\zeta')]\,\nabla(z+\Psi) \\ \nabla \cdot \mathbf{q}(\boldsymbol{x}) = 0. \end{cases} \tag{7}$$

Due to the random nature of Y' and ζ', the system (7) becomes stochastic, and we aim at computing the statistical moments of the FVs. To solve (7), we expand Ψ, $\mathbf{q}$, $\exp(Y')$ and $\exp(\zeta')$ in asymptotic-series as follows

$$\Psi = \Psi_0 + \Psi_1 + \Psi_2 + \ldots; \quad \mathbf{q} = \mathbf{q}^{(0)} + \mathbf{q}^{(1)} + \mathbf{q}^{(2)} + \ldots; \quad \exp(Y') = 1 + \frac{Y'}{1!} + \frac{Y'^2}{2!} + \ldots; \quad \exp(\zeta') = 1 + \frac{\zeta'}{1!} + \frac{\zeta'^2}{2!} + \ldots \tag{8}$$

The nonlinear term $f(\Psi, \zeta') \equiv \exp[\Psi\exp(\zeta')]$ appearing into the first of (7) is likewise expanded up to the second-order, i.e.,

$$\begin{aligned} f(\Psi, \zeta') = f(\Psi_0, 0) + \frac{1}{1!}\left[\frac{\partial}{\partial\Psi_1} f(\Psi, \zeta')|_{(\Psi_0,0)} \Psi_1(\boldsymbol{x}) + \frac{\partial}{\partial\zeta'} f(\Psi, \zeta')|_{(\Psi_0,0)} \zeta'(\boldsymbol{x})\right] + \frac{\partial}{\partial\Psi_2} f(\Psi, \zeta')|_{(\Psi_0,0)} \Psi_2(\boldsymbol{x}) \\ + \frac{\partial}{\partial\zeta'^2} f(\Psi, \zeta')|_{(\Psi_0,0)} \zeta'^2(\boldsymbol{x}) + \frac{1}{2!}\left[\frac{\partial}{\partial\Psi_1} f(\Psi, \zeta')|_{(\Psi_0,0)} \Psi_1(\boldsymbol{x}) + \frac{\partial}{\partial\zeta'} f(\Psi, \zeta')|_{(\Psi_0,0)} \zeta'(\boldsymbol{x})\right]^{(2)} + \ldots. \end{aligned} \tag{9}$$

To compute the first-order derivatives of $f(\Psi, \zeta')$ at the right-hand side of (9), we employ the chain-rule of derivation, i.e.,

$$\frac{\partial}{\partial\Psi_1} f(\Psi, \zeta')|_{(\Psi_0,0)} = \left[\frac{\mathrm{d}}{\mathrm{d}\Psi} f(\Psi, \zeta') \cdot \frac{\partial\Psi}{\partial\Psi_1}\right]_{(\Psi_0,0)} = [\exp(\zeta') f(\Psi, \zeta') \cdot 1]_{(\Psi_0,0)} = K_r(\Psi_0), \tag{10a}$$

$$\frac{\partial}{\partial\zeta'} f(\Psi, \zeta')|_{(\Psi_0,0)} = \left[\frac{\mathrm{d}f(\Psi, \zeta')}{\mathrm{d}\exp(\zeta')} \cdot \frac{\partial\exp(\zeta')}{\partial\zeta'}\right]_{(\Psi_0,0)} = \left[\Psi f(\Psi, \zeta') \cdot \frac{1}{1!}\right]_{(\Psi_0,0)} = \Psi_0(z) K_r(\Psi_0), \tag{10b}$$

$$\frac{\partial}{\partial\Psi_2} f(\Psi, \zeta')|_{(\Psi_0,0)} = \left[\frac{\mathrm{d}}{\mathrm{d}\Psi} f(\Psi, \zeta') \cdot \frac{\partial\Psi}{\partial\Psi_2}\right]_{(\Psi_0,0)} = [\exp(\zeta') f(\Psi, \zeta') \cdot 1]_{(\Psi_0,0)} = K_r(\Psi_0), \tag{10c}$$

$$\frac{\partial}{\partial\zeta'^2}f(\Psi,\zeta')|_{(\Psi_0,0)}=\left[\frac{\mathrm{d}f(\Psi,\zeta')}{\mathrm{d}\exp(\zeta')}\cdot\frac{\partial\exp(\zeta')}{\partial\zeta'^2}\right]_{(\Psi_0,0)}=\left[\Psi f(\Psi,\zeta')\cdot\frac{1}{2!}\right]_{(\Psi_0,0)}=\frac{1}{2}\,\Psi_0(z)\,K_r(\Psi_0), \tag{10d}$$

where hereafter we shall set: $K_r(\Psi_0)\equiv\exp(\Psi_0)$. The second-order derivatives are computed by means of (10a)–(10b), the final result being:

$$\frac{\partial^2}{\partial\Psi_1^2}f(\Psi,\zeta')|_{(\Psi_0,0)}=\left[\frac{\partial}{\partial\Psi_1}\frac{\partial}{\partial\Psi_1}f(\Psi,\zeta')\right]_{(\Psi_0,0)}=\left[\exp(\zeta')\frac{\partial}{\partial\Psi_1}f(\Psi,\zeta')\right]_{(\Psi_0,0)}=K_r(\Psi_0), \tag{11a}$$

$$\begin{aligned}\frac{\partial^2 f(\Psi,\zeta')}{\partial\Psi_1\partial\zeta'}|_{(\Psi_0,0)}&=\left\{\frac{\partial}{\partial\Psi_1}\left[\frac{\partial}{\partial\zeta'}f(\Psi,\zeta')\right]\right\}_{(\Psi_0,0)}=\left\{\frac{\partial}{\partial\Psi_1}[\Psi f(\Psi,\zeta')]\right\}_{(\Psi_0,0)}=\\&=\left[f(\Psi,\zeta')\frac{\partial\Psi}{\partial\Psi_1}+\Psi\frac{\partial}{\partial\Psi_1}f(\Psi,\zeta')\right]_{(\Psi_0,0)}=f(\Psi_0,0)+\Psi_0\left[\frac{\partial}{\partial\Psi_1}f(\Psi,\zeta')\right]_{(\Psi_0,0)}=K_r(\Psi_0)+\Psi_0K_r(\Psi_0),\end{aligned} \tag{11b}$$

$$\frac{\partial^2}{\partial\zeta'^2}f(\Psi,\zeta')|_{(\Psi_0,0)}=\left[\frac{\partial}{\partial\zeta'}\frac{\partial}{\partial\zeta'}f(\Psi,\zeta')\right]_{(\Psi_0,0)}=\Psi_0\left[\frac{\partial}{\partial\zeta'}f(\Psi,\zeta')\right]_{(\Psi_0,0)}=\Psi_0^2K_r(\Psi_0). \tag{11c}$$

To summarize, the asymptotic-expansion of the constitutive-law reads as:

$$\begin{aligned}\mathbf{q}(\boldsymbol{x})=&-K_r(\Psi_0)\nabla[z+\Psi_0(z)+\Psi_1(\boldsymbol{x})+\Psi_2(\boldsymbol{x})+\ldots]\left[1+Y'(\boldsymbol{x})+\frac{1}{2}Y'^2(\boldsymbol{x})+\ldots\right]\times\\&\left\{1+\Psi_2(\boldsymbol{x})+\Psi_1(\boldsymbol{x})+\Psi_0(z)\zeta'(\boldsymbol{x})+\Psi_1(\boldsymbol{x})\zeta'(\boldsymbol{x})+\frac{\Psi_0(z)}{2}\zeta'^2(\boldsymbol{x})+\frac{1}{2}[\Psi_1(\boldsymbol{x})+\Psi_0(z)\zeta'(\boldsymbol{x})]^2+\ldots\right\}.\end{aligned} \tag{12}$$

We wish to note that a more general result, i.e., accounting for any functional shape $K_r\equiv K_r(\Psi)$, can be found in *Indelman et al*. [1993]. However, for the functional model (5) one easily recovers from *Indelman et al*. [1993] the same linearized expression (12).

2.1. The Leading-Order Approximation

At the zero-order the system (7) writes as

$$\begin{cases}\mathbf{q}^{(0)}(\boldsymbol{x})=-K_r(\Psi_0)\,\nabla(z+\Psi_0)\\ \nabla\cdot\mathbf{q}^{(0)}(\boldsymbol{x})=0\end{cases}\quad\Rightarrow\quad\nabla\cdot[K_r(\Psi_0)\nabla\Psi_0]+\frac{\partial}{\partial z}K_r(\Psi_0)=0 \tag{13}$$

with the following boundary conditions:

$$\Psi_0(\boldsymbol{x})|_{z=0}=0,\qquad K_r(\Psi_0)\left(1+\frac{\partial}{\partial z}\Psi_0\right)\Big|_{z=L}=-q_0. \tag{14}$$

To solve the boundary-value problem (13)–(14), we employ a modified Kirchhoff transformation

$$\mathcal{F}(\boldsymbol{x})=\exp\left(\frac{z}{2}\right)\int_{-\infty}^{\Psi_0}\mathrm{d}s\,K_r(s)=\exp\left(\frac{z}{2}\right)K_r(\Psi_0) \tag{15}$$

[*Severino and Tartakovsky*, 2015] to map the second of (13) into an Helmholtz-type equation

$$\nabla^2\mathcal{F}(\boldsymbol{x})-\frac{1}{4}\mathcal{F}(\boldsymbol{x})=0, \tag{16}$$

whereas the boundary-conditions (14) become:

$$\mathcal{F}(\boldsymbol{x})|_{z=0}=1,\qquad\frac{\partial}{\partial z}\mathcal{F}(\boldsymbol{x})+\frac{1}{2}\mathcal{F}(\boldsymbol{x})\Big|_{z=L}=-q_0\exp(L/2). \tag{17}$$

Skipping the straightforward algebraic derivations, one ends up with

$$\mathbf{q}^{(0)}=q_0\,\boldsymbol{e}_z,\qquad\Psi_0(z)=\ln\{-q_0[1-\kappa\exp(-z)]\},\qquad\kappa=1+q_0^{-1}. \tag{18}$$

Note that the zero-order terms $\mathbf{q}^{(0)}$ and Ψ_0 are function of the vertical coordinate z solely, since the boundary conditions (17) do not depend upon the planar coordinate $\boldsymbol{x}_h\equiv(x,y)\in\mathbb{R}^2$. Moreover, one can easily check that: $0\le-q_0[1-\kappa\exp(-z)]\le1$ (it is reminded that $-1\le q_0\le0$, and concurrently $-\infty<\kappa\le0$),

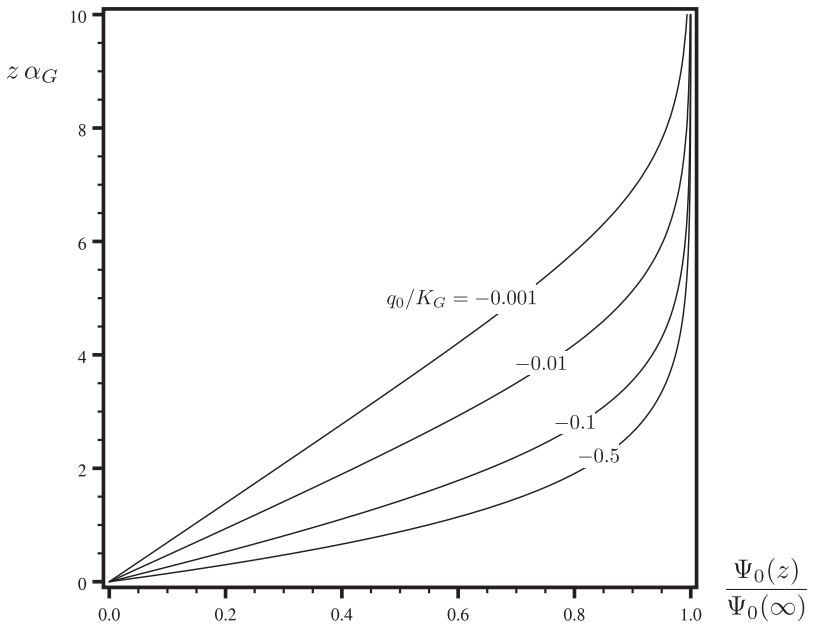

Figure 2. The normalized leading order pressure head $\Psi_0(z)/\Psi_0(\infty)$ as function of the scaled depth $z\,\alpha_G$, and different values of the non-dimensional flux q_0/K_G.

therefore implying that $\Psi_0 \in]-\infty, 0]$ [*Severino and Coppola*, 2012]. Finally, away from the water table it yields: $\Psi_0 \approx \ln(-q_0) \equiv \Psi_0(\infty)$, in agreement with previous studies dealing with an unbounded flow-domain [see, e.g., *Russo*, 1993; *Severino and Santini*, 2005; *Severino et al*., 2009]. In the Figure 2, the leading order pressure $\Psi_0(z)$ relative to its far field $\Psi_0(\infty)$ has been depicted along $z\,\alpha_G$ for several values of the normalized flux q_0/K_G. The high sensitivity of Ψ_0 to the infiltrating flux q_0 is clearly seen. In particular, the smaller q_0/K_G, the larger the distance (from the water table $z = 0$) of attainment the far field, and vice versa.

2.2. The First-Order Approximation

At the first order the mass-conservation and the constitutive law write as

$$\nabla \cdot \mathbf{q}^{(1)}(\boldsymbol{x}) = 0, \qquad \mathbf{q}^{(1)}(\boldsymbol{x}) = -K_r(\Psi_0)\nabla\Psi_1(\boldsymbol{x}) + q_0[\Psi_1(\boldsymbol{x}) + Y'(\boldsymbol{x}) + \Psi_0(z)\,\zeta'(\boldsymbol{x})]\boldsymbol{e}_z, \tag{19}$$

where we have accounted for the fact that $-K_r(\Psi_0)\nabla(z+\Psi_0) \equiv q_0\boldsymbol{e}_z$. By combining equation (19), one obtains the governing equation for the fluctuation Ψ_1 of the pressure-head, i.e.,

$$\nabla[K_r(\Psi_0)\nabla\Psi_1(\boldsymbol{x})] - q_0\frac{\partial}{\partial z}\Psi_1(\boldsymbol{x}) = q_0\frac{\partial}{\partial z}[Y'(\boldsymbol{x}) + \Psi_0(z)\zeta'(\boldsymbol{x})] \tag{20}$$

which, due to the deterministic nature of the pressure head at the water table, is solved with zero-boundary conditions.

Equation (20) represents the starting point to obtain the statistical moments of interest. In particular, moments can be computed by either solving for Ψ_1 (and subsequently averaging) or via the MME. In the present study, it was found easier in terms of mathematical derivations to follow this second avenue. Note that for large z it yields $K_r(\Psi_0) \approx -q_0$, and one recovers from (20) the same equation of *Severino and Santini* [2005] valid for an unbounded domain.

2.3. The Second-Order Approximation

The second-order correction to the flux is derived similarly to the previous case, the final result being:

$$\nabla \cdot \mathbf{q}^{(2)}(\boldsymbol{x}) = 0, \quad \mathbf{q}^{(2)}(\boldsymbol{x}) = -K_r(\Psi_0)\nabla\Psi_2(\boldsymbol{x}) + q_0\Psi_2(\boldsymbol{x})\boldsymbol{e}_z - K_r(\Psi_0)[\Psi_1(\boldsymbol{x}) + Y'(\boldsymbol{x}) + \Psi_0(z)\,\zeta'(\boldsymbol{x})]\nabla\Psi_1(\boldsymbol{x}) +$$
$$+ q_0\left\{\frac{1}{2}[\Psi_1(\boldsymbol{x}) + \Psi_0(z)\zeta'(\boldsymbol{x})]^2 + \Psi_1(\boldsymbol{x})Y'(\boldsymbol{x}) + \Psi_1(\boldsymbol{x})\zeta'(\boldsymbol{x}) + \frac{1}{2}Y'^2(\boldsymbol{x}) + \Psi_0(z)Y'(\boldsymbol{x})\zeta'(\boldsymbol{x}) + \frac{\Psi_0(z)}{2}\zeta'^2\right\}\boldsymbol{e}_z. \tag{21}$$

Elimination of $\mathbf{q}^{(2)}$ into (21) leads to the following equation for the second-order approximation Ψ_2 of the pressure-head:

$$\nabla \cdot [K_r(\Psi_0)(z)\nabla\Psi_2(\boldsymbol{x})] - q_0 \frac{\partial}{\partial z}\Psi_2(\boldsymbol{x}) = q_0 \frac{\partial}{\partial z}\mathcal{L}_2(\boldsymbol{x}) - \mathcal{L}_2'(\boldsymbol{x}), \tag{22}$$

where we have set

$$\begin{aligned}\mathcal{L}_2(\boldsymbol{x}) \equiv \Psi_1(\boldsymbol{x})Y'(\boldsymbol{x}) + \Psi_0(z)Y'(\boldsymbol{x})\zeta'(\boldsymbol{x}) + \frac{1}{2}\Psi_0(z)\zeta'^2(\boldsymbol{x}) + \Psi_1(\boldsymbol{x})\zeta'(\boldsymbol{x}) + \frac{1}{2}Y'^2(\boldsymbol{x}) + \\ + \frac{1}{2}[\Psi_1(\boldsymbol{x}) + \Psi_0(z)\zeta'(\boldsymbol{x})]^2 - q_0^{-1}K_r(\Psi_0)[\Psi_1(\boldsymbol{x}) + Y'(\boldsymbol{x}) + \Psi_0(z)\zeta'(\boldsymbol{x})]\frac{\partial}{\partial z}\Psi_1(\boldsymbol{x}),\end{aligned} \tag{23}$$

$$\mathcal{L}_2'(\boldsymbol{x}) \equiv K_r(\Psi_0)\nabla_h\{[\Psi_1(\boldsymbol{x}) + Y'(\boldsymbol{x}) + \Psi_0(z)\zeta'(\boldsymbol{x})]\nabla_h\Psi_1(\boldsymbol{x})\}, \qquad \nabla_h \equiv \left(\frac{\partial}{\partial x}, \frac{\partial}{\partial y}\right). \tag{24}$$

It is important to notice that, since all the RSFs appearing into (24) are stationary in horizontal plane, it results $\langle \mathcal{L}_2'(\boldsymbol{x})\rangle = 0$.

3. Second-Order Moments of the Pressure-Head

Before proceeding with the derivation of the second-order moments of Ψ, it is worth noting that, due to the linear dependence (see equation (20)) of Ψ_1 upon Y' and ζ' in the plane of isotropy, the various moments will result stationary RSFs there. Furthermore, since we are interested in the unsaturated flow close to the water table ($z = 0$), we can regard the soil surface ($z = L$) sufficiently far away from such a zone, so that one can let $L \to \infty$. Note that this latter assumption does not modify the leading-order expressions (18) of the FVs. In addition, away from the water table $z = 0$ the lower boundary condition does not impact anymore, and consequently the FVs tend to become stationary, unless the upper boundary condition (i.e., the soil's surface) is approached (in this latter case the flow would again result nonstationary).

We start from the two-point covariances $C_{\Psi\gamma}(\boldsymbol{x}, \boldsymbol{x}')$ whose governing equation is obtained by multiplying (20) by γ evaluated at $\boldsymbol{x}' \neq \boldsymbol{x}$ and averaging, i.e.,

$$\mathcal{L}\, C_{\Psi\gamma}(\boldsymbol{x}, \boldsymbol{x}') = q_0 \frac{\partial}{\partial z}\left[C_{Y\gamma}(\boldsymbol{x} - \boldsymbol{x}') + \Psi_0(z)C_{\zeta\gamma}(\boldsymbol{x} - \boldsymbol{x}')\right], \qquad \mathcal{L} \equiv \nabla\{K_r[\Psi_0(z)]\nabla\} - q_0\frac{\partial}{\partial z} \tag{25}$$

where, by virtue of the stationarity of the soil-properties, we have set $\langle Y'(\boldsymbol{x})\,\gamma(\boldsymbol{x}')\rangle \equiv C_{Y\gamma}(\boldsymbol{x} - \boldsymbol{x}')$ and similarly for $\langle \zeta'(\boldsymbol{x})\,\gamma(\boldsymbol{x}')\rangle$. Hereafter, we shall assume that the ensemble average $\langle \mathcal{A}\rangle$ of any RSF $\mathcal{A}$ is interchangeable with its spatial counterpart $\overline{\mathcal{A}}$, i.e., $\langle \mathcal{A}\rangle \simeq \overline{\mathcal{A}}$ (ergodic hypothesis). We also adopt in the sequel the following convention: $Y\gamma \equiv Y$ for $\gamma = Y$, and $\zeta\gamma \equiv \zeta$ for $\gamma = \zeta$. To facilitate the successive derivations, it is useful to introduce the transformation

$$C_{\Psi\gamma}(\boldsymbol{x}, \boldsymbol{x}') = \sqrt{-q_0}\,\frac{\exp(-z/2)}{K_r[\Psi_0(z)]}\,\Phi(\boldsymbol{x}, \boldsymbol{x}') \tag{26}$$

which converts (25) into an Helmholtz-type problem:

$$\nabla^2\Phi(\boldsymbol{x}, \boldsymbol{x}') - \frac{1}{4}\Phi(\boldsymbol{x}, \boldsymbol{x}') = -\sqrt{-q_0}\exp\left(\frac{z}{2}\right)\frac{\partial}{\partial z}\left[C_{Y\gamma}(\boldsymbol{x} - \boldsymbol{x}') + \Psi_0(z)C_{\zeta\gamma}(\boldsymbol{x} - \boldsymbol{x}')\right]. \tag{27}$$

For the sake of simplicity, we limit to quote the final result

$$C_{\Psi\gamma}(r_h, z, z') = g(z)\int_0^\infty \mathrm{d}k\, kJ_0(kr_h)\int_0^\infty \mathrm{d}\xi\,\chi_\gamma(\xi)\,\frac{\mathrm{d}}{\mathrm{d}\xi}\left[\exp\left(\frac{\xi}{2}\right)G_\beta(z, \xi)\right], \quad g(z) \equiv \frac{\exp(-z/2)}{1 - \kappa\exp(-z)} \tag{28}$$

$$\chi_\gamma(\xi) = \sigma_{Y\gamma}\,\tilde{\rho}_h(kl_{Y\gamma})\,\rho_v\left(\frac{\xi - z'}{\tilde{\lambda}_{Y\gamma}}\right) + \sigma_{\zeta\gamma}\,\tilde{\rho}_h(kl_{\zeta\gamma})\,\Psi_0(\xi)\,\rho_v\left(\frac{\xi - z'}{\tilde{\lambda}_{\zeta\gamma}}\right), \tag{29}$$

$$G_\beta(z, \xi) = \beta^{-1}\left[\exp\left(-\frac{z + \xi}{2}\beta\right) - \exp\left(-\frac{|z - \xi|}{2}\beta\right)\right], \qquad \beta = \sqrt{1 + 4k^2} \tag{30}$$

and address the interested reader to Appendix A for details. In equation (28) J_0 is the zero-order Bessel

function of the first kind, r_h is the magnitude of the vector $(x-x', y-y')$, and $\bar{\lambda}_\mu \equiv \lambda_\mu I_\mu$ (no summation-convention). The expression (28) is a general representation of the cross-covariances $C_{\Psi\gamma}$, and its computation is achieved by carrying out two quadratures. The cross-variance $\sigma_{\Psi\gamma}(z)$ is derived by setting $r_h = 0$ and $z \equiv z'$ into (28).

The head covariance C_Ψ is obtained multiplying (20) by $\Psi_1(\boldsymbol{x}')$, and averaging:

$$\mathcal{L}\, C_\Psi(\boldsymbol{x}, \boldsymbol{x}') = q_0 \frac{\partial}{\partial z}[C_{\Psi Y}(\boldsymbol{x}', \boldsymbol{x}) + \Psi_0(z) C_{\Psi\zeta}(\boldsymbol{x}', \boldsymbol{x})]. \tag{31}$$

Notice that the cross-covariances $C_{\gamma\Psi}(\boldsymbol{x}, \boldsymbol{x}')$ were replaced by $C_{\Psi\gamma}(\boldsymbol{x}', \boldsymbol{x})$ since maintaining the order between $\boldsymbol{x}$ and $\boldsymbol{x}'$ is crucial due to the nonstationarity of $C_{\gamma\Psi}$ along the depth. The solution for C_Ψ is achieved similarly to the previous case, and the final result is (Appendix A):

$$C_\Psi(r_h, z, z') = g(z) g(z') \int_0^\infty \mathrm{d}k\, k\, J_0(k\, r_h) \int_0^\infty \int_0^\infty \mathrm{d}\xi\, \mathrm{d}\eta\, \Sigma(\xi, \eta) \frac{\partial^2}{\partial\xi \partial\eta} \left[\exp\left(\frac{\xi+\eta}{2}\right) G_\beta(z, \xi) G_\beta(z', \eta) \right] \tag{32}$$

$$\begin{aligned} \Sigma(\xi, \eta) = {} & \sigma_Y^2 I_Y \tilde{\rho}_h(k I_Y) \rho_v\left(\frac{\xi-\eta}{\bar{\lambda}_Y}\right) + \sigma_{Y\zeta} I_{Y\zeta}\, \tilde{\rho}_h(k I_{Y\zeta}) [\Psi_0(\xi) + \Psi_0(\eta)] \rho_v\left(\frac{\xi-\eta}{\bar{\lambda}_{Y\zeta}}\right) + \\ & + \sigma_\zeta^2\, I_\zeta\, \tilde{\rho}_h(k I_\zeta)\, \Psi_0(\xi)\, \Psi_0(\eta)\, \rho_v\left(\frac{\xi-\eta}{\bar{\lambda}_\zeta}\right). \end{aligned} \tag{33}$$

Likewise, the head variance $\sigma_\Psi^2 \equiv \sigma_\Psi^2(z)$ is obtained by setting $r_h = 0$, and $z \equiv z'$ into (32).

4. Higher-Order Correction of the Mean Pressure-Head

To compute the higher-order correction $\langle\Psi\rangle = \Psi_0 + \langle\Psi_2\rangle$ of the mean head, one has to solve the equation (22) for the second-order correction Ψ_2. Like before, such a task is easily achieved by means of the transformation $\Psi_2(\boldsymbol{x}) = \sqrt{-q_0}\, \frac{\exp(-z/2)}{K_r[\Psi_0(z)]}\, \Phi_2(\boldsymbol{x})$ which casts (22) into an Helmholtz equation, i.e.,

$$\nabla^2 \Phi_2 - \frac{1}{4}\, \Phi_2 = -\sqrt{-q_0} \exp\left(\frac{z}{2}\right) \left[\frac{\partial}{\partial z} \mathcal{L}_2(\boldsymbol{x}) - q_0^{-1} \mathcal{L}_2'(\boldsymbol{x}) \right]. \tag{34}$$

Taking the ensemble average into (34) provides the equation for $\langle\Phi_2\rangle$, i.e.,

$$\frac{\mathrm{d}^2}{\mathrm{d}z^2} \langle\Phi_2(z)\rangle - \frac{1}{4} \langle\Phi_2(z)\rangle = -\sqrt{-q_0} \exp\left(\frac{z}{2}\right) \frac{\mathrm{d}}{\mathrm{d}z} \langle\mathcal{L}_2(z)\rangle, \tag{35}$$

$$\begin{aligned} \langle\mathcal{L}_2(z)\rangle = {} & \frac{1}{2}\sigma_Y^2 + \Psi_0(z)\sigma_{Y\zeta} + \frac{\Psi_0(z)}{2}[1 + \Psi_0(z)]\sigma_\zeta^2 + \sigma_{\Psi Y}(z) + [1 + \Psi_0(z)]\sigma_{\Psi\zeta}(z) + \\ & + \frac{1}{2}\sigma_\Psi^2(z) - \frac{1}{q_0} K_r(\Psi_0) \left[\frac{1}{2} \frac{\mathrm{d}}{\mathrm{d}z} \sigma_\Psi^2(z) + \langle Y'(\boldsymbol{x}) \frac{\partial}{\partial z} \Psi_1(\boldsymbol{x}) \rangle + \Psi_0(z) \langle \zeta'(\boldsymbol{x}) \frac{\partial}{\partial z} \Psi_1(\boldsymbol{x}) \rangle \right], \end{aligned} \tag{36}$$

where we have accounted for the fact that $\langle\mathcal{L}_2'(\boldsymbol{x})\rangle = 0$. Notice that, due to the stationarity of the term $\mathcal{L}_2$ in the horizontal-plane (see equation (23)), the function $\langle\Phi_2\rangle$ (and concurrently $\langle\Psi_2\rangle$) depends upon the depth z, solely. A similar conclusion was drawn both by *Zhang and Winter* [1998] via extensive MCs, and by [*Indelman et al.*, 1993] by means of analytical tools. Thus, solving for $\langle\Phi_2\rangle$ and back substitution leads to

$$\langle\Psi_2(z)\rangle = \frac{1}{f_\kappa(z)} \left\{ \langle\mathcal{L}_2(\infty)\rangle [1 - \exp(-z)] - \exp(-z) \int_0^z \mathrm{d}\xi \exp(\xi)\, \langle\mathcal{L}_2(\xi)\rangle \right\}, \quad f_\kappa(z) = 1 - \kappa \exp(-z). \tag{37}$$

It is convenient to represent the mean pressure-head as $\langle\Psi(z)\rangle = \Psi_0(z) + \langle\Psi_2(z)\rangle = \Psi_0(z)\, \Theta(z)$, where we have set $\Theta(z) = 1 + \psi(z)$ with

$$\psi(z) = \frac{\langle\Psi_2(z)\rangle}{\Psi_0(z)} = q_0 \frac{\exp[-\Psi_0(z)]}{\Psi_0(z)} \left\{ \exp(-z) \int_0^z \mathrm{d}\xi \exp(\xi)\, \langle\mathcal{L}_2(\xi)\rangle - \langle\mathcal{L}_2(\infty)\rangle [1 - \exp(-z)] \right\}. \tag{38}$$

The utility of such a representation is that $\langle\Psi\rangle$ is expressed via the product between Ψ_0 (valid for a homogeneous formation) and a characteristic function Θ which "modifies" Ψ_0 according to the medium's heterogeneity. One advantage related to the representation $\langle\Psi(z)\rangle = \Psi_0(z)\, \Theta(z)$ is that it is instrumental to identify the statistical properties of a vadose zone. Indeed, once $\langle\Psi\rangle$ has been estimated by the

measurements of the pressure-heads at different locations, one can identify the statistical parameters pertaining to the RSFs Y, $Y\zeta$, and ζ by matching against to it.

The general expression of the normalized correction ψ allows one to investigate the flow behavior in the near and far field. More precisely, at large depths one has $\psi(\infty)=0$, and concurrently $\langle\Psi(\infty)\rangle \equiv \Psi_0(\infty)[1+\psi(\infty)]=\ln(-q_0)$, which coincides with the result obtained by *Russo* [1993], and *Severino and Santini* [2005] in the case of an unbounded domain. Instead, at the water table ($z=0$) it is easily shown from (38) (we omit the algebraic derivations) that: $\psi(0)=[\langle\mathcal{L}_2(\infty)\rangle-\langle\mathcal{L}_2(0)\rangle]/\kappa<\infty$, and therefore we recover that: $\langle\Psi(0)\rangle \equiv \Psi_0(0)[1+\psi(0)]=0$. This result is explained by noting that the boundary condition at $z=0$ requires a fixed head, and thus the heterogeneity does not affect the value of the pressure-head there (see also discussion in *Severino and Coppola* [2012]). These two asymptotics can be useful: (i) in the practical applications (to design proper sampling-strategies), and (ii) in the modeling aspects (to validate more involved numerical codes).

5. Calibration Versus Validation

We wish here to illustrate the application/use of the theoretical results obtained so far. In particular, it is seen that a relatively large number of input parameters, i.e., geometric means of the saturated conductivity and the alpha-parameter as well as the related (cross)-covariances, has to be preliminarily selected. While the statistical characterization of Y and ζ has been largely discussed and assessed (see e.g., the survey exploited in *Rubin*, [2003], and references therein), the cross-correlation Y–ζ is still a matter of debate, and it deserves a thorough analysis. To this end, we refer to a recently conducted unsaturated flow experiment in a field [*Severino et al*., 2010, 2016a, 2016b], which is described briefly herein with special care to the identification of the statistical quantities which are relevant for the present study.

The field is located at the Ponticelli-site (Naples, Italy). The soil texture was analyzed by sampling at several (randomly selected) locations across the field. The resulting structure is that of a typical "andosol": a structureless sand with a small (lesser than a coarse-textured soil) bulk density $\varrho=(1.0\pm0.1)\,\mathrm{g/cm^3}$ [*Terribile et al*., 2007; *Comegna et al*., 2013]. Prior to any analysis concerning the spatial distribution, it is instrumental to examine the measurements of Y and ζ by means of conventional (univariate) statistics.

5.1. Univariate Analysis of Y and ζ

The saturated conductivity K_s was measured (by a permeameter working at constant head) upon ~80 samples taken at two depths along a transect 50 m-long (1.25 m horizontal step) excavated parallel to the experimental site. The measure of α was instead acquired in the field by means of an internal test drainage (a general description about such a test as well as the identification procedure can be found in *Severino et al*. [2003]; *Gómez et al*., [2009]). More precisely, the field was pounded by applying water in excess of the infiltration rate. After 2 days of continuous ponding (when steady state conditions were almost reached) water's application was halted, and monitoring initiated. This latter consisted of simultaneous measurements of the water content ϑ and the pressure head Ψ (taken by TDR-probes and tensiometers, respectively) at three depths, $z=0.30,\ 0.60,\ 0.90$ m (from the soil surface), along the transect. Monitoring was interrupted 77 days later, when drainage was evolving too slowly to make it impossible to further collect significantly different pairs of (ϑ,Ψ). The experimental hydraulic conductivity curve $K^{(\mathrm{ex})} \equiv K^{(\mathrm{ex})}(\Psi)$ was determined by following the method suggested by *Basile et al*. [2003]. Hence, the value of α was determined by matching the theoretical curve $K_r \equiv K_r(\Psi)$ (second of equation (5)) against to $K^{(\mathrm{ex})}(\Psi)$ divided by the K_s-value measured upon the sample taken at the same depth (details can be found in *Comegna et al*. [2006]).

Table 1. Estimates of the: (i) Mean, (ii) Standard Deviation, and (iii) Coefficient of Variation Together With the D -Test of Normal (Null) Hypothesis[a]

Statistics	$Y \equiv \ln K_s$	$\zeta \equiv \ln\alpha$
Mean	2.30	−3.31
Standard deviation	1.38	$2.76\cdot10^{-1}$
Coefficient of variation	$6.01\cdot10^{-1}$	$8.35\cdot10^{-2}$
D -test (0.895)*	0.882	0.715

[a]For comparison purposes, the reference value at the 5%-level of confidence is in the circular brackets. Values of K_s and α are expressed in cm/h and $\mathrm{cm^{-1}}$.

The empirical (symbols) *cumulative distribution function* (CDF) of $Y \equiv \ln K_s$ (blue) and $\zeta \equiv \ln\alpha$ (red) along with the theoretical (continuous) fitted normal CDFs are shown in the Figure 3. The observed good agreement between empirical and theoretical CDFs is quantitatively confirmed by the *Kolmogorov-Smirnov* test (Table 1). To summarize, both ζ and Y can be considered as

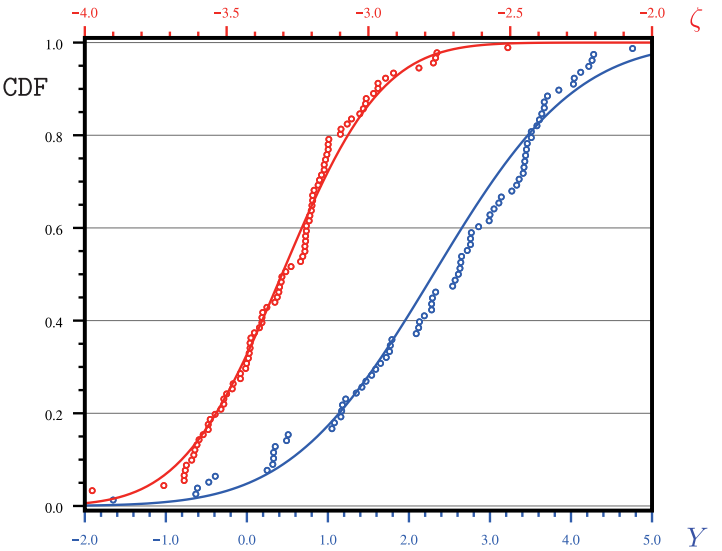

Figure 3. Cumulative distribution functions of measured (symbols) $Y \equiv \ln K_s$ (blue) and $\zeta \equiv \ln \alpha$ (red). Continuous lines represent the respective fitted theoretical CDFs. The saturated conductivity K_s and the α-parameter are expressed in cm/h and cm^{-1}, respectively.

normally distributed with the latter exhibiting a larger variability than the former. It is worth noting that the intervals of (5%)-confidence of the quantity $(\sigma_u/\mu_u)^2$ (being u either K_s or α) as determined (i) by the raw u-data, and (ii) by the expression $\exp(\sigma^2_{\ln u})-1$ (which is known to apply to log-normally distributed random variables) are:

Thus, the overlapping between the intervals of confidence further demonstrates that the log-transforms of K_s and α can be regarded (up to the experimental errors) as normally distributed random variables.

In order to investigate possible scale-issues, the saturated conductivity K_s was measured in the field (Auger-hole device), as well. The intervals of 5%-confidence (see Table 2) for the estimates of the mean and variance of $Y \equiv \ln K_s$ demonstrate that there is no statistical difference between the characterization of Y at laboratory and at field scale. This is explained by recalling that the sampling volume of the Auger-hole device is approximately of the same size (details are in *Severino et al.* [2010]) of the soil samples (see also discussion in *Fallico et al.* [2016]). The usefulness of using laboratory K_s-measurements stems from the fact that these were more numerous than those at field scale (Table 3).

Likewise, the support volumes attached to the devices (i.e., time domain reflectometry, and piezometers) used in situ to detect the pairs (θ, Ψ) at the several locations are approximately of the same size of the soil samples taken from the site [see *Comegna et al.*, 2013]. As a consequence, the measurements of the α-parameter can be regarded de facto as local ones (comparable with those of K_s at laboratory scale). Of course, matters would result completely different if one aims at inferring the statistics of α (or of any other random variable) by using the ensemble average of the flow variables [see, e.g., *Severino et al.*, 2003]. In this case, due to the completely different size of the involved volume support, the comparison between local and field scale measurements should also account for the proper upscaling [see, e.g., *Russo*, 2003; *Severino and Santini*, 2005; *Severino and Coppola*, 2012].

To investigate whether ζ and Y can be considered cross-correlated, we have used the Student's t test with $t \simeq r_{\zeta Y}\sqrt{(n-2)/(1-r^2_{\zeta Y})}$, being $r_{\zeta Y}$ the estimate of the correlation coefficient, i.e.,

$$r_{\zeta Y} \equiv \frac{\sigma_{\zeta Y}}{\sigma_\zeta\, \sigma_Y} \simeq \frac{\sum_i (\zeta_i - \bar{\zeta})(Y_i - \bar{Y})}{\sqrt{\left(\sum_i \zeta_i^2\right)\left(\sum_i Y_i^2\right)}} = 0.143, \qquad (i = 1, \cdots, 82). \tag{39}$$

Since it yields $t = 1.292$ ($n = 82$), the null hypothesis (H_0: $\rho_{\zeta Y} \equiv 0$) cannot be rejected till to the 10% of confidence (it is remained that $1.292 \simeq t_{0.10}$). The residuals (ζ', Y') along with the regression-line and the 95% confidence-limits are displayed in Figure 4. The weak correlation, which is detected at a first glance (by the modest slope of the regression-line), is also confirmed by the *Fisher*-test (p-value ~5.72 %). However, for the experiment at stake, such a correlation is not statistically significative (at the 5% of confidence). The same findings were observed into similar

Table 2. Intervals of (5%)-Confidence of $(\sigma_u/\mu_u)^2$ as Determined by the u-Data, and by the Expression $\exp(\sigma^2_{\ln u})-1$

$(\sigma_u/\mu_u)^2$	$\ln K_s$	$\ln \alpha$
u-data	$[0, 697; 2, 32]$	$[5, 27; 10, 4] \cdot 10^{-2}$
$\exp(\sigma^2_{\ln u})-1$	$[1, 59; 9, 85]$	$[5, 38; 10, 5] \cdot 10^{-2}$

Table 3. Intervals of 5%-Confidence for the Estimates of the Mean and Variance of Y at Laboratory and Field Scale

Scale	$\langle Y \rangle$	σ_Y^2	Number of Data
Laboratory	$(199; 261) \cdot 10^{-2}$	$(142; 267) \cdot 10^{-2}$	82
Field	$(227; 293) \cdot 10^{-2}$	$(150; 287) \cdot 10^{-2}$	70

previous studies [*Wierenga et al.*, 1991; *Russo and Bouton*, 1992; *Russo et al.*, 1997].

More generally, even if a positive correlation may result important for the variance of the unsaturated conductivity $K \equiv K(\Psi)$ [see, e.g., *Russo et al.*, 1997], it is worth noting here that, into studying the impact upon the flow and transport processes, one can still regard (along the lines suggested by *Russo and Bouton* [1992]) $Y \equiv \ln K_s$ and $\zeta \equiv \ln \alpha$ as uncorrelated random fields (the weak positive correlation notwithstanding). More important is the fact that in coarser-textured soils (like the one at the Ponticelli site) the cross correlation is found of scarce importance [see, e.g., *Ragab and Cooper*, 1993a, 1993b; *Tartakovsky et al.*, 1999]. Finally, in the case of the Ponticelli site, the α-parameter can be regarded as a given constant (see below), and this further underpins the neglect of the Y–ζ correlation. Thus, for all these reasons we feel comfortable disregarding the cross correlation between K_s and α.

Though our general theory allows one dealing with a variance of ζ of the same order of that of Y, the soil properties of the Ponticelli site (see Table 1) show that $\sigma_\zeta^2/\sigma_Y^2 = \mathcal{O}(10^{-2})$, and therefore one can disregard the variability of the former as compared with that of the latter. This is tantamount to assume α everywhere equal to α_G. Hence, we can limit our analysis to the zero-order approximation in σ_ζ, and to the second-order approximation in σ_Y.

5.2. Spatial Heterogeneity-Structure of Y

The problem of quantifying the spatial structure (autocorrelation) of Y is rather complicated, even when measurements are numerous. The procedure should involve several steps: (i) an hypothesis about the functional model of the covariance, (ii) estimates of the parameters of such a model, and (iii) a model validation test [see, e.g., *Russo and Bouton*, 1992; *Russo et al.*, 1997]. The problem of selecting the most appropriate model remains to some extent in the realm of the practical applications [*Rubin*, 2003]. The prevailing approach is the pragmatic one: select a model for its practicality/versatility as well as its performance in similar situations, determine the parameter(s), and check subsequently its usefulness by matching against to real data. Thus, by adopting this stand point, and in line with the model structure (6), for the horizontal autocorrelation (for simplicity hereafter denoted by ρ_h) we select the Gaussian model, i.e.,

$$\rho_h(x_h) \equiv \exp\left[-\pi\left(\frac{x_h}{2I}\right)^2\right] \tag{40}$$

(with $I_Y \equiv I$). Hence, the horizontal integral scale was estimated by considering the two sampling depths, separately (Figure 5). The results were nevertheless quite similar leading to $I \sim 20$ m. Note that the relatively large value of the horizontal integral scale I is not surprising due to the stratified nature of the vadose zone at stake, and it significantly differs from its other counterparts [e.g., *Russo and Bouton*, 1992; *Russo et al.*, 1997]. It has to be noted that, given the ratio $L/I \simeq (50\ \text{m})/(20\ \text{m})$ between the transect length-scale L and I, the flow domain cannot be regarded "into a strict sense" as ergodic. In fact, only when the flow domain is large enough with respect to the integral scales of the RSF, the spatial average of the single (available) realization can be replaced with the ensemble mean. Otherwise, the spatial average is only an estimate of the ensemble mean, which in turn is affected by uncertainty. In particular, for a domain of finite size such an uncertainty increases with both the coefficient of variation and the size of the integral scales of the spatially variable hydraulic properties.

However, a previous study conducted by *Comegna and Basile* [1994] about the spatial distribution of the soil hydraulic properties in the same site (and involving a much larger domain) has led to a similar statistical characterization. Thus, given this extra information, we feel comfortable about the fact that the domain at the Ponticelli site can be regarded as approximately ergodic. Last, as it will be clearer later on, the good matching between theoretical and experimental values provides (among the others) a posteriori justification of the presumed ergodicity (the numerous approximations, source of uncertainties, and measurement-errors notwithstanding).

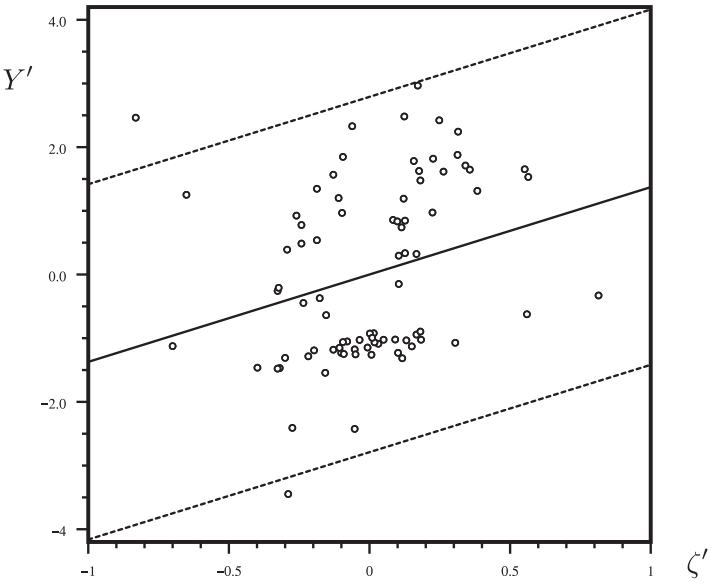

Figure 4. Residuals of Y versus residuals of ζ. The linear regression and the associated 95% confidence-limits are represented by solid and dashed lines, respectively.

To complete the spatial characterization of Y at the Ponticelli site, the vertical autocorrelation (hereafter denoted by ρ_v) has to be identified. However, the scarce availability of K_s-measurements along the vertical does not enable one to identify ρ_v by the same procedure which we used for the horizontal autocorrelation. Thus, we used geological information to gain insight about the shape of ρ_v. More precisely, the analysis of the texture suggests that the soil is a sedimentary structureless sand [*Severino et al*., 2010]. This is also confirmed by the geological pattern of the formation: subsequent depositions of different (erupted) materials [*Comegna et al*., 2010], and therefore the soil can be sought as a collection of sedimentary lenses each one exhibiting different Y-values from one lense to the other. This is a typical feature of those formations where the vertical correlation scale is found to be much lesser than the horizontal one [*Russo and Bresler*, 1981]. In this case the soil property is characterized by a complete lack of vertical correlation, thus authorizing to replace the vertical autocorrelation with a Dirac distribution, i.e., $\rho_v \sim \delta$. Such an approximation (also known as δ-correlation) was adopted in previous studies pertaining to both the vadose zone [e.g., *Indelman et al*., 1993; *Severino and Santini*, 2005; *Severino and Coppola*, 2012], and the aquifers [e.g., *Fiori et al*., 1998; *Indelman and Dagan*, 1999; *Severino*, 2011b; *Severino et al*., 2012b; *Severino and Bartolo*, 2015]. We apply the statistical characterization obtained by dealing with the first meters to the entire flow domain (∼40 m). Such a choice is justified on the basis of the available geological

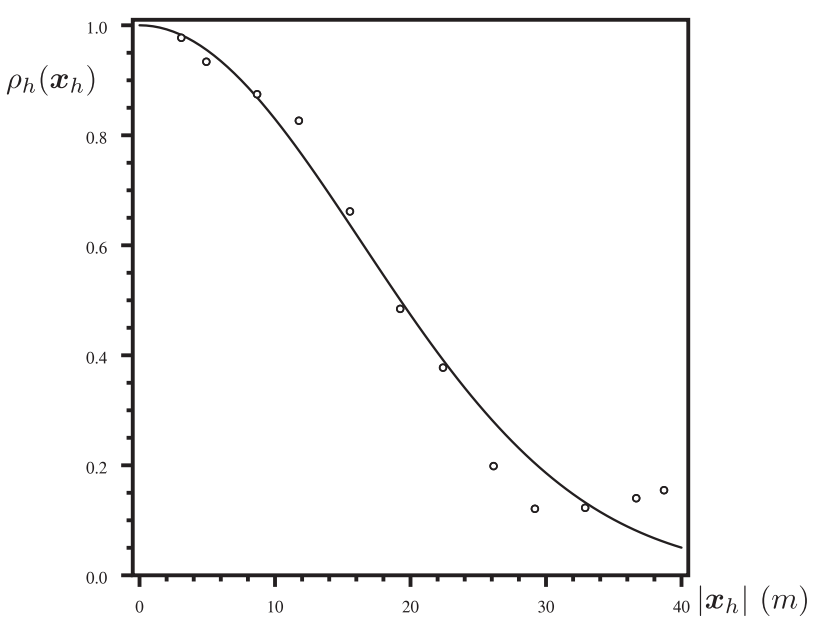

Figure 5. Horizontal autocorrelation function for the log-conductivity Y. Symbols pertain to the measured values, whereas the continuous line refers to the Gaussian model (40) with $I \equiv 20.5$ m.

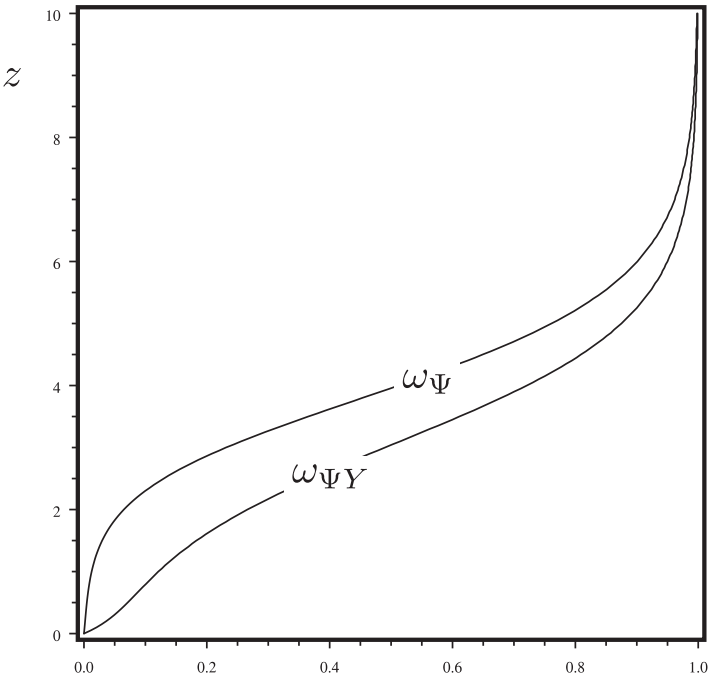

Figure 6. Dependence of the weight-functions (horizontal axe) $\omega_{\Psi Y}$–ω_Ψ upon the depth z (normalized by $\alpha_G^{-1}=27.4$ cm). The parameter κ associated to the infiltrating non dimensional flux ($q_0=-4.21\cdot10^{-2}$) is $\kappa=1+q_0^{-1}=-22.8$.

information [*Terribile et al.*, 2007] suggesting that the soil at stake can be thought as a continuous sequence of thin stratified (mainly erupted) materials of the same type of those detected at the shallow depths. At any rate, from a general point of view, it is reminded that any statistical characterization of the soil's hydraulic properties based upon shallow measurements is not enough for the entire flow domain. A rigorous (methodological) approach would require a dense sampling campaign at all the depths (similarly to *Russo and Bouton* [1992]; *Russo et al.* [1997]).

With the input parameters and the autocorrelation functions identified so far, we are in position to compute the (cross)-variances $\sigma_{\Psi Y}$ and σ_Ψ^2. By omitting the (very lengthy) algebraic derivations, the final result is:

$$\sigma_{\Psi Y}(z)=\sigma_{\Psi Y}(\infty)\frac{\mathcal{F}_{\Psi Y}(z)}{f_\kappa(z)},\qquad \sigma_\Psi^2(z)=\sigma_\Psi^2(\infty)\frac{\mathcal{F}_\Psi(z)}{f_\kappa^2(z)} \tag{41}$$

$$\mathcal{F}_{\Psi Y}(z)=1-\frac{\Lambda(2z)}{\Lambda(0)}(1+2\pi z^2)+\frac{2z}{\Lambda(0)}\exp(-z), \tag{42}$$

$$\mathcal{F}_\Psi(z)=1-\frac{\Lambda(2z)}{\Lambda(0)}\{1+2\pi z[1-\exp(-z)]\}+\frac{2}{\Lambda(0)}[\exp(-z)-\exp(-2z)], \tag{43}$$

being $\Lambda(a)=\exp\left[\frac{1+(\pi a)^2}{4\pi}\right]\mathrm{erfc}\left(\frac{1+\pi a}{2\sqrt{\pi}}\right)$, whereas $\sigma_{\Psi Y}(\infty)=-\frac{\Lambda(0)}{2}\lambda I\sigma_Y^2$ and $\sigma_\Psi^2(\infty)=\frac{\Lambda(0)}{2}\lambda(I\sigma_Y)^2$ are the far field (large z) values of (41). Note that we have set $\lambda_Y\equiv\lambda$, for simplicity. It is seen that the functions $\omega_{\Psi Y}(z)\equiv\sigma_{\Psi Y}(z)/\sigma_{\Psi Y}(\infty)$ and $\omega_\Psi(z)\equiv\sigma_\Psi^2(z)/\sigma_\Psi^2(\infty)$ are weights driving the transition (see Figure 6) of the (cross)variance (41) from the water table, where $\omega_{\Psi Y}(0)=\omega_\Psi(0)=0$, to the far field, where $\omega_{\Psi Y}(\infty)=\omega_\Psi(\infty)=1$. Note that the rate of the transition from the water table to the far field with the infiltration flux q_0 is regulated by the term $f_\kappa\equiv f_\kappa(z)$, solely. Due to its multiplicative structure, the quantity $\kappa\exp(-z)$ is significantly different from zero only when $z\ll1$, i.e., close to the water table. To the contrary, away from the water table (i.e., $z\gg1$) one has $f_\kappa\sim1$, in agreement with *Severino and Santini* [2005].

Table 4. Steady-State Values of the Experimental Spatial: (i) Mean, $\overline{\Psi}$, of the Pressure Head; (ii) Cross-Variance, $\bar{\sigma}_{\Psi Y}$; (iii) Head-Variance, $\bar{\sigma}_\Psi^2$; and (iv) Number of Samples, N, at the Three Sampling Depths Lying at: (i) $z=40.0-0.9=39.1$m (the Deepest), (ii) $z=40.0-0.6=39.4$m (Intermediate), and (iii) $z=40.0-0.9=39.7$m (the Shallowest) Above the Water Table Which Is 40 m Deep[a]

$z(-)$	$\overline{\Psi}(-)$	$\bar{\sigma}_{\Psi Y}(-)$	$\bar{\sigma}_\Psi^2(-)$	N
145	−3.60	$-6.88\cdot10^{-2}$	7.60	35
144	−2.87	$-9.55\cdot10^{-2}$	12.3	37
143	−2.52	$-1.30\cdot10^{-1}$	15.5	36

[a]Moments, i.e., $\bar{\sigma}_{\Psi Y}$ – $\bar{\sigma}_\Psi^2$, and depths, i.e., z, have been made dimensionless by adopting $\alpha_G^{-1}=27.4\,cm$ as length scale.

We are now in position to complete the characterization of the heterogeneity structure of the field at stake by identifying the anisotropy ratio λ by means of the variance σ_Ψ^2 of the pressure head. This implies that the steady state Ψ-measurements are required, and therefore before going further it is worth exploiting the experimental

Table 5. Lower, i.e., $\overline{\Psi}_{\text{lower}} \equiv \overline{\Psi} - \bar{\sigma}_\Psi/\sqrt{N}$, and Upper, i.e., $\overline{\Psi}_{\text{upper}} \equiv \overline{\Psi} + \bar{\sigma}_\Psi/\sqrt{N}$, Limit of the Interval of Confidence of the Mean Pressure Head as Determined From Data at the Three Sampling Depths (Table 2), Along With the Asymptotic Mean Value $\Psi_0(\infty) \equiv \ln(-q_0) = \ln(4.21 \cdot 10^{-2})$[a]

z	$\overline{\Psi}_{\text{lower}}$	$\Psi_0(\infty)$	$\overline{\Psi}_{\text{upper}}$
145	−4.1	−3.2	−3.1
144	−3.5	−3.2	−2.3
143	−3.2	−3.1	−1.9

[a]Pressure-head values and depths have been made dimensionless by adopting $\alpha_G^{-1} = 27.4$ cm as length scale.

data set which has been used for such a purpose. Indeed, during another stage of the experimental campaign (aiming to monitor a solute transport process), the plot was irrigated ($4.2 \cdot 10^{-1}$ cm/h) until stationary (steady) values of the pressure head Ψ (and water content, as well) were detected at the sampling depths along the trench. By this time, pressure-head values were read at the tensiometers along the trench, and the statistical (dimensionless) moments, which are of interest for the present study, are summarized in the Table 4.

Since the sampling depths lie very far from the water table (details are in the caption of Table 4), it yields from Figure 6 that $\omega_\Psi(z) \simeq \omega_\Psi(\infty) \equiv 1$, and concurrently one can use the asymptotic value of the head variance to estimate the anisotropy ratio λ. The legitimacy of using the asymptotic $\sigma_\Psi^2(\infty)$ for calibration purposes is corroborated by the fact that the far field $\Psi_0(\infty)$ of the mean head lies within the interval of confidence of the mean pressure-heads (Table 5). The anisotropy ratio λ is approximately $2.4 \cdot 10^{-3}$. It is interesting to note that such an estimate implies that $I_v = \lambda I \sim 5$ cm, a value which is in line with the geological information [*Comegna et al.*, 2010] about the thickness of the strata, i.e., $\mathcal{O}(10\text{ cm})$, detected at the experimental site.

In the Figure 7 we have depicted the far field value of the pressure-head variance (continuous red line) as calibrated by means of the experimental (red symbols) values. In the same figure, we also compare the far field cross variance (continuous black line) against to the experimental (black symbols) values which were not used for the above calibration. Note that the deviations of the experimental far field $\sigma_{\Psi Y}$ and σ_Ψ^2 from their theoretical (i.e., constant) counterparts lie within the errors of measurements of the tensiometers [*Comegna et al.*, 2006, 2010]. Thus, the matching between theoretical and experimental $\sigma_{\Psi Y}$ represents a satisfactory validating benchmark.

After determining all the relevant quantities required by the flow model, we are in position to make predictions upon the behavior of the FVs in the close vicinity of the water table. To this end, we wish to point out here that direct measurements would have been tremendously time consuming and expensive, and most

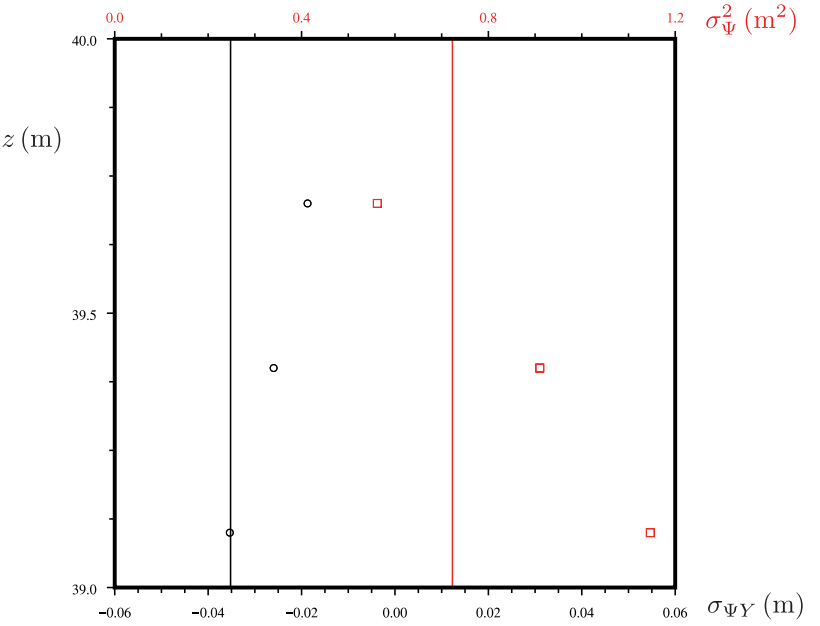

Figure 7. Distribution of the cross-variance $\sigma_{\Psi Y}$ (black), and the head-pressure variance σ_Ψ^2 (red) along the depth z (from the water table). Symbols refer to the experimental measurements, whereas continuous lines pertain to the far field values of (41).

of them probably even impossible since the water table is 40 m deep. This further underpins the usefulness of our model to predict the behavior of flow (and transport) variables by relating shallow measurements (which can be carried out with a relatively ease) to depths of the vadose zone which are practically unaccessible.

6. Discussion

We wish to illustrate how the developed stochastic model can be used to grasp the behavior of the flow variables close to the water table. The input parameters are those determined by the set of real data pertaining to the Ponticelli site (Naples, Italy).

Due to its importance in the applications (e.g., quantifying the recharge of the aquifers and/or determining the solute mass arrivals at the water table), we mainly concentrate the present discussion upon the uncertainty qualification of flux $\mathbf{q}$ along the depth z. To compute the variance of this latter, the starting point is the first-order approximation (19), which is rewritten here as

$$\mathbf{q}^{(1)}(\boldsymbol{x}) \simeq -K_r(\Psi_0)\nabla\Psi_1(\boldsymbol{x})+q_0[\Psi_1(\boldsymbol{x})+Y'(\boldsymbol{x})]\boldsymbol{e}_z, \tag{44}$$

to account for the approximations which we have shown to be valid for the Ponticelli-site. To derive the variance of the flux in the horizontal plane, we take advantage from the stationarity of the flow variables there. Thus, we write the horizontal component $\mathbf{q}_h^{(1)}$ of the fluctuation (44) by means of its spectral (Fourier transform) representation, i.e.,

$$\mathbf{q}_h^{(1)}(\boldsymbol{x}_h,z)={}_JK_r(z)\int\frac{\mathrm{d}\boldsymbol{k}}{2\pi}\boldsymbol{k}\,\tilde{\Psi}_1(\boldsymbol{k},z)\exp\left(-{}_J\boldsymbol{k}\cdot\boldsymbol{x}_h\right) \tag{45}$$

being

$$\tilde{\Psi}_1(\boldsymbol{k},z)=-q_0\,\frac{\exp(-z/2)}{K_r(z)}\int_0^\infty \mathrm{d}\xi\,\tilde{Y}'(\boldsymbol{k},\xi)\,\frac{\mathrm{d}}{\mathrm{d}\xi}\left[\exp\left(\frac{\xi}{2}\right)G_\beta(z,\xi)\right] \tag{46}$$

the horizontal (2D) Fourier transform of the pressure-head fluctuation. For ease of notation, we have set $K_r(\Psi_0)\equiv K_r(z)$. Taking the square of (45), and accounting for the property

$$\langle\tilde{Y}'(\boldsymbol{k}_1,z_1)\,\tilde{Y}'(\boldsymbol{k}_2,z_2)\rangle=2\pi\lambda\,\sigma_Y^2\delta(\boldsymbol{k}_1+\boldsymbol{k}_2)\tilde{\rho}_h(k_2)\delta(z_1-z_2) \tag{47}$$

leads (after introducing polar coordinates) to:

$$\sigma_{q_h}^2(z)=\lambda(q_0\sigma_Y)^2\exp(-z)\int_0^\infty \mathrm{d}k\,k^3\tilde{\rho}_h(k)\,\mathcal{G}_\beta(z,z), \tag{48}$$

$$\mathcal{G}_\beta(z,\zeta)\equiv\int_0^\infty \mathrm{d}\xi\,\frac{\mathrm{d}}{\mathrm{d}\xi}\left[\exp\left(\frac{\xi}{2}\right)G_\beta(z,\xi)\right]\frac{\mathrm{d}}{\mathrm{d}\xi}\left[\exp\left(\frac{\xi}{2}\right)G_\beta(\zeta,\xi)\right]. \tag{49}$$

Note that, due to the stationarity of the flux in the isotropy (horizontal) plane, the variance (48) does not depend upon x_h. To compute $\mathcal{G}_\beta(z,z)$, we preliminarily note that upon integrating by parts in (49) it yields

$$\mathcal{G}_\beta(z,\zeta)=-\int_0^\infty \mathrm{d}\xi\exp\left(\frac{\xi}{2}\right)G_\beta(z,\xi)\frac{\mathrm{d}^2}{\mathrm{d}\xi^2}\left[\exp\left(\frac{\xi}{2}\right)G_\beta(\zeta,\xi)\right]. \tag{50}$$

Then, by recalling that $G_\beta(\zeta,\xi)$ is such that $\frac{\mathrm{d}^2}{\mathrm{d}\xi^2}G_\beta(\zeta,\xi)-\frac{\beta^2}{4}G_\beta(\zeta,\xi)=\delta(\xi-\zeta)$, one has

$$\frac{\mathrm{d}^2}{\mathrm{d}\xi^2}\left[\exp\left(\frac{\xi}{2}\right)G_\beta(\zeta,\xi)\right]=\exp\left(\frac{\xi}{2}\right)\left[\frac{\beta^2+1}{4}\,G_\beta(\zeta,\xi)+\frac{\mathrm{d}}{\mathrm{d}\xi}G_\beta(\zeta,\xi)+\delta(\xi-\zeta)\right], \tag{51}$$

and therefore substitution into the last of (50) gives

$$\mathcal{G}_\beta(z,\zeta)=-\exp(\zeta)G_\beta(z,\zeta)-\frac{\beta^2+1}{4}\int_0^\infty \mathrm{d}\xi\exp(\xi)G_\beta(z,\xi)G_\beta(\zeta,\xi)-\int_0^\infty \mathrm{d}\xi\exp(\xi)G_\beta(z,\xi)\frac{\mathrm{d}}{\mathrm{d}\xi}G_\beta(\zeta,\xi). \tag{52}$$

The function $\mathcal{G}_\beta(z,z)$ is now computed by taking the limit $\zeta\to z$ into (52), i.e.,

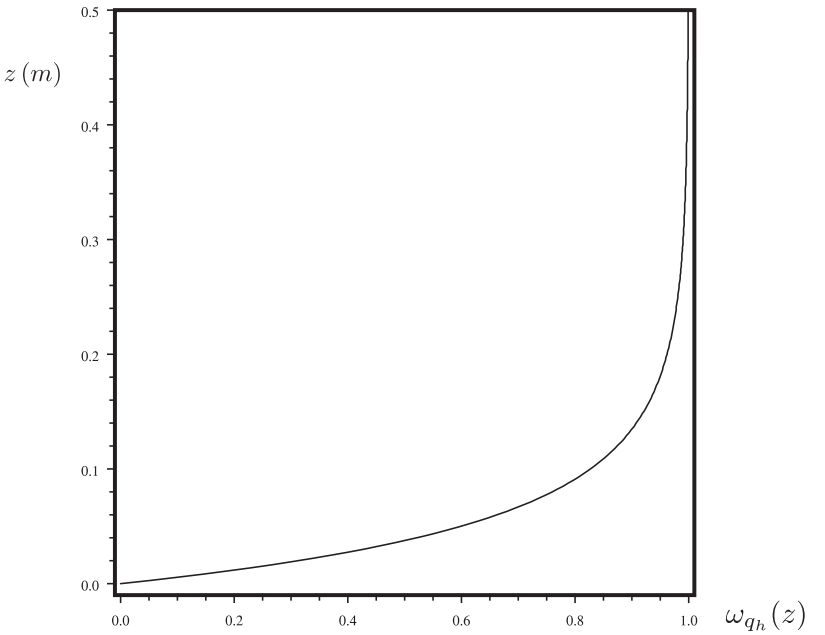

Figure 8. Dependence of the weight function $\omega_{q_h} \equiv \omega_{q_h}(z)$ (horizontal axe) upon the dimensional depth z (vertical axe).

$$\mathcal{G}_\beta(z,z) = \lim_{\zeta \to z} \mathcal{G}_\beta(z,\zeta) = -\exp(z) G_\beta(z,z) - \frac{\beta^2+1}{4} \int_0^\infty \mathrm{d}\xi \exp(\xi) G_\beta^2(z,\xi) - \frac{1}{2} \int_0^\infty \mathrm{d}\xi \exp(\xi) \frac{\mathrm{d}}{\mathrm{d}\xi} G_\beta^2(z,\xi), \quad (53)$$

and carrying out integration by parts in the last integral, to have

$$\mathcal{G}_\beta(z,z) = -\exp(z) G_\beta(z,z) - \frac{\beta^2-1}{4} \int_0^\infty \mathrm{d}\xi \exp(\xi) G_\beta^2(z,\xi). \quad (54)$$

Evaluation of the straightforward integral on the right hand side of (54) leads to

$$\mathcal{G}_\beta(z,z) = \frac{1}{2} \{\exp(z)[\beta+2-2\exp(-\beta z)] - \beta \exp(-\beta z)\}. \quad (55)$$

Hence, the variance (48) reads as

$$\sigma_{q_h}^2(z) = \sigma_{q_h}^2(\infty)\, \omega_{q_h}(z), \qquad \omega_{q_h}(z) \equiv 1 - \exp(-z) + 2z \frac{(4\pi^2 z^2 + 6\pi - 1)\Lambda(2z) + 2(1-2\pi z)\exp(-z)}{14 + (6\pi - 1)\Lambda(0)}, \quad (56)$$

being $\sigma_{q_h}^2(\infty) = \frac{\pi}{8}[14 + (6\pi-1)\Lambda(0)]\lambda(q_0\, \sigma_Y)^2$ the far field (large z). Like above, it is seen (Figure 8) that the function $\omega_{q_h} \equiv \omega_{q_h}(z)$ is a depth-dependent weight describing the transition of $\sigma_{q_h}^2(z)$ from the water table, where $\omega_{q_h}(0) \equiv 0$, till to its far field, corresponding to $\omega_{q_h}(\infty) \equiv 1$. It is interesting to note that $\sigma_{q_h}^2 \neq 0$ (for $z > 0$) although the mean flux is purely vertical everywhere in the flow domain. This is due to the fact that, unlike the mean, the fluctuation of the flux (and therefore the variance) has a three-dimensional structure. Instead, the vanishing of $\sigma_{q_h}^2$ at the water table ($z = 0$) is explained by the deterministic nature of the head there which requires $\tilde{\Psi}_1(\boldsymbol{k}, 0) \equiv 0$ (see (45)–(46)).

The variance $\sigma_{q_z}^2 \equiv \langle q_z^{(1)2} \rangle$ of the vertical flux is computed by the same token. Thus, starting from the fluctuation

$$q_z^{(1)}(\boldsymbol{x}) = -K_r(z) \frac{\partial}{\partial z} \Psi_1(\boldsymbol{x}) + q_0[\Psi_1(\boldsymbol{x}) + Y'(\boldsymbol{x})], \quad (57)$$

the variance of the vertical flux reads as

$$\sigma^2_{q_z}(z)=K_r^2(z)\langle\frac{\partial}{\partial z}\Psi_1(\boldsymbol{x})\frac{\partial}{\partial z}\Psi_1(\boldsymbol{x})\rangle+q_0^2\left[\sigma^2_Y+2\,\sigma_{\Psi Y}(z)+\sigma^2_\Psi(z)\right]-2\,q_0\,K_r(z)\left[\frac{1}{2}\frac{\mathrm{d}}{\mathrm{d}z}\,\sigma^2_\Psi(z)+\langle Y'(\boldsymbol{x})\frac{\partial}{\partial z}\Psi_1(\boldsymbol{x})\rangle\right]. \tag{58}$$

To compute the two still left ensemble averages, we make use of the spectral representation of (46), i.e.,

$$\Psi_1(\boldsymbol{x}_h,z)\equiv\int\frac{\mathrm{d}\boldsymbol{k}}{2\pi}\exp\left(-\imath\boldsymbol{k}\cdot\boldsymbol{x}_h\right)\tilde{\Psi}_1(\boldsymbol{k},z)=g(z)\int_0^\infty\mathrm{d}\xi\int\frac{\mathrm{d}\boldsymbol{k}}{2\pi}\exp\left(-\imath\boldsymbol{k}\cdot\boldsymbol{x}_h\right)\tilde{Y}'(\boldsymbol{k},\xi)\,\frac{\mathrm{d}}{\mathrm{d}\xi}\left[\exp\left(\frac{\xi}{2}\right)G_\beta(z,\xi)\right] \tag{59}$$

leading to

$$\left\langle\frac{\partial}{\partial z}\Psi_1(\boldsymbol{x})\frac{\partial}{\partial z}\Psi_1(\boldsymbol{x})\right\rangle=\lambda\,\sigma^2_Y g^2(z)\left[\mathcal{L}^2(z)\,\Upsilon(z,\zeta)+2\,\mathcal{L}(z)\frac{\partial}{\partial\zeta}\,\Upsilon(z,\zeta)+\frac{\partial^2}{\partial z\partial\zeta}\,\Upsilon(z,\zeta)\right]_{\zeta\equiv z} \tag{60}$$

$$\langle Y'(\boldsymbol{x})\frac{\partial}{\partial z}\Psi_1(\boldsymbol{x})\rangle=\frac{\lambda\,\sigma^2_Y}{4\,f_\kappa(z)}\mathcal{F}(z), \tag{61}$$

$$\mathcal{F}(z)=[4+\Lambda(2z)-\Lambda(0)]\mathcal{L}(z)+\pi\left[\left(1+2z+2\pi z^2\right)\Lambda(2z)+\Lambda(0)\right]-(1+2\pi z)\exp\left(-z\right)-5, \tag{62}$$

where $\mathcal{L}(z)\equiv\frac{\mathrm{d}}{\mathrm{d}z}\ln\left[g(z)\right]=-\frac{1+\kappa\exp\left(-z\right)}{2[1-\kappa\exp\left(-z\right)]}$, and $\Upsilon(z,\zeta)\equiv\int_0^\infty\mathrm{d}k\,k\,\rho_h(k)\,\mathcal{G}_\beta(z,\zeta)$. It is therefore clear that the crux of the matter to derive the variance (58) is the computation of the Υ-function as well as its derivatives. With the details in Appendix B, equation (58) reads as

$$\frac{\sigma^2_{q_z}(z)}{(q_0\,\sigma_Y)^2}=1+2\frac{\sigma_{\Psi Y}(z)}{\sigma^2_Y}+\frac{\sigma^2_\Psi(z)}{\sigma^2_Y}\left[1+f_\kappa(z)\frac{\mathrm{d}}{\mathrm{d}z}\ln\sigma^2_\Psi(z)\right]-\frac{\lambda}{8}\left[4\mathcal{L}^2(z)\Upsilon_1(z)+4\mathcal{L}(z)\Upsilon_2(z)+\Upsilon_3(z)-4\mathcal{F}(z)\right], \tag{63}$$

being the Υ_i-functions given in equations (B6 and B7) of Appendix B. In particular, the far and near field of $\sigma^2_{q_z}$ are:

$$\frac{\sigma^2_{q_z}(\infty)}{(q_0\,\sigma_Y)^2}=1-\frac{\lambda}{4}\left[11+7\pi+\frac{3}{2}(2\pi^2-\pi+1)\Lambda(0)\right],\qquad\frac{\sigma^2_{q_z}(0)}{(q_0\,\sigma_Y)^2}=1-\frac{\lambda}{4}[14-\pi\Lambda(0)], \tag{64}$$

respectively. It is seen that $\sigma^2_{q_z}(\infty)<\sigma^2_{q_z}(0)$ which is due to the fact that at the groundwater ($z=0$) particles move much more freely (due to the absence of retention there) as compared with the unsaturated zone,

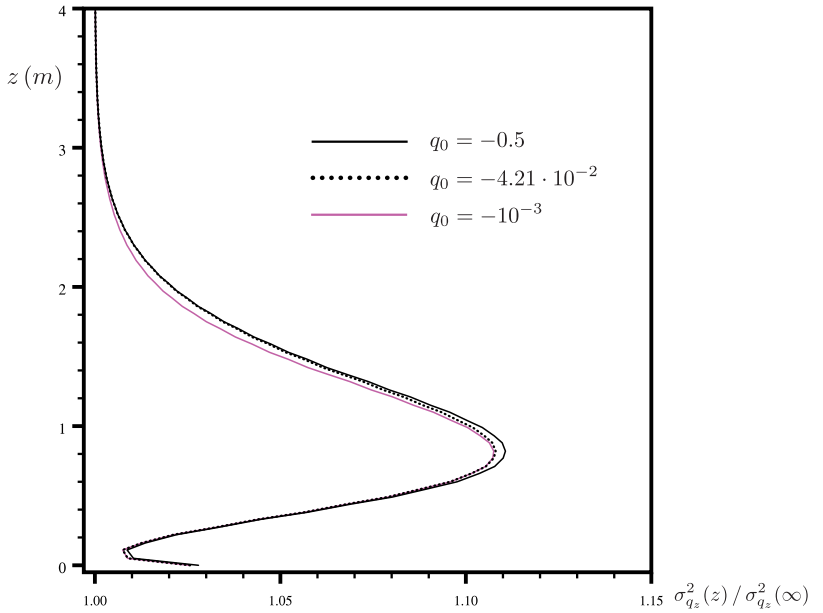

Figure 9. Normalized variance $\sigma^2_{q_z}(z)/\sigma^2_{q_z}(\infty)$ of the vertical specific flux as a function of the (dimensional) depth from the water table under a few values of the dimensionless infiltration rate q_0. Thick dot-line pertains to the normalized infiltration rate during the experiment at the Ponticelli site.

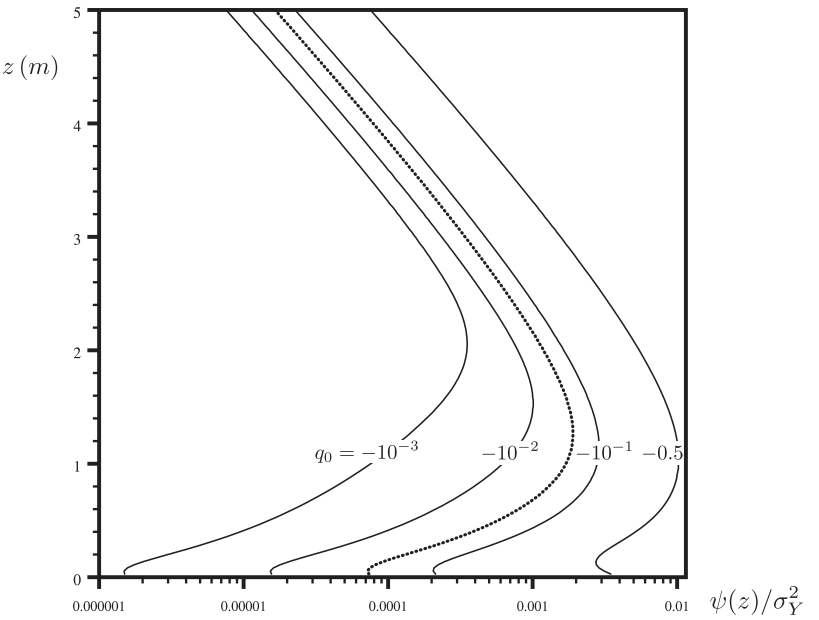

Figure 10. Distribution of the scaled head-factor $\psi(z)/\sigma_Y^2$ as computed from (38), and accounting for the data of the Ponticelli site along the dimensional depth z from the water table ($z = 0$), and a few values of the dimensionless infiltration rate q_0. Thick dot-line pertains to the normalized infiltration rate (i.e., $q_0 = -4.21 \cdot 10^{-2}$) during the experiment at the Ponticelli site.

and concurrently particles experience larger deviation from the mean vertical velocity, therefore giving rise to a larger variance. The normalized variance $\sigma^2_{q_z}(z)/\sigma^2_{q_z}(\infty)$ of the vertical specific flux along z (expressed in m) is depicted in the Figure 9. Close to the water table the fluctuation $\Psi^{(1)}$ of the pressure head undergoes to the largest variations, as it is clearly detected by the pattern of ω_Ψ in the Figure 6, and concurrently so does (see (44)) the fluctuation $q_z^{(1)} \equiv q_z - q_z^{(0)}$. This explains why the major source of uncertainty (i.e., large $\sigma^2_{q_z}$) of the vertical flux is concentrated next above the water table. Such an out-coming is also in agreement with the large time limit of the numerical results of *Ferrante and Yeh* [1999]. Furthermore, it is worth reminding that the infiltrating flux q_0 is the upper boundary condition that, being at $z \to \infty$, does not significantly impact the behavior of the variance of the vertical specific flux at $z = 0$. This explains the scarce sensitivity of $\sigma^2_{q_z}$ to the infiltrating flux q_0 close to the water table (see also the discussion in *Wang et al.* [2009]. To quantify the distortion effect upon the mean head $\langle\Psi\rangle$ as determined by the heterogeneity of the Ponticelli's soil, in the Figure 10 we have depicted the quantity $\psi(z)/\sigma_Y^2$ versus the (dimensional) depth from the water table. Results show that ψ decreases with decreasing q_0. In particular, the result:

$$\psi(0) = -\sigma_Y^2 \frac{\lambda}{2\kappa}\left[\pi\Lambda(0) + \frac{1+\kappa}{1-\kappa}\right] > \psi(\infty) \equiv 0 \tag{65}$$

(it is reminded that $\kappa \leq 0$) is explained by the fact that close to the water table the pressure head attains the highest values, and therefore ψ results larger than its far field. It is worth reminding that a utility of the definition (38) is that one can filter out from the second-order correction $\langle\Psi_2(z)\rangle$ the impact of the zero-order one Ψ_0, this latter being highly sensitive to the influx q_0 (see Figure 2), and concurrently ψ accounts exclusively for the heterogeneity of the vadose zone. This explains the slight dependence of $\psi \equiv \psi(z)$ (Figure 10) upon the magnitude q_0. Of course, to recover the effective dependence of $\langle\Psi_2(z)\rangle$ upon the infiltration flux, the depth, and the medium's heterogeneity, one has to consider the product $\psi(z)\Psi_0(z)$.

The distance at which stationarity is reached is roughly 3 m, similarly to $\sigma^2_{q_z}$ (see Figure 9). An analogous conclusion was achieved by *Zhang and Winter* [1998]. An important (often overlooked) question is about the asymptotic nature of the perturbation expansions (8). In fact, for the perturbation expansion $\langle\Psi\rangle = \Psi_0 + \langle\Psi_2\rangle$ to be asymptotic, it is necessary that $\langle\Psi_2\rangle \ll \Psi_0$, a condition which, from equation (38), is equivalent to $\psi \ll 1$. Hence, it is seen (Figure 10) that $\psi/\sigma_Y^2 \lesssim 10^{-2}$ (any z and q_0), and therefore, as far as the heterogeneity of Y is accounted for, our solution for $\langle\Psi\rangle$ is accurate till to $\sigma_Y^2 = \mathcal{O}(1)$. In other words, although the perturbation expansion (8) is nominally restricted to mildly heterogeneous vadose zones, it works de facto quite well for relatively highly heterogeneous unsaturated porous formations (in analogy to what is observed in the aquifers, see e.g., *Fiori et al.* [2010]). Similar conclusions were drawn by *Tartakovsky et al.* [1999] for a one-dimensional vadose zone.

7. Conclusions

We have developed a stochastic model for three-dimensional steady flows in the vadose zone accounting for the presence of the water table. The system the governing equations is solved at first-order of approximation in the variances of the log-transforms of: (i) the saturated conductivity K_s, and (ii) the α-parameter of the *Gardner* [1958] model. Very general expression of the statistical (second-order) moments of the pressure head and specific flux are then obtained. These moments are expressed into analytical (closed form) expression which can be easily evaluated once the statistical structure of the above soil parameters is specified. One of the main result of the present paper is the general representation $\langle\Psi\rangle=\Psi_0(z)\Theta(z)$ with $\Theta(z)=1+\psi(z)$. The term ψ has been derived in a closed form which is easily evaluated after specifying the shape of the various correlation functions (6). In particular, it is shown that at large distances one has $\psi(\infty)=0$, and concurrently $\langle\Psi(\infty)\rangle\equiv\ln(-q_0)$, which coincides with the result valid for an unbounded vadose zone. Instead, at the water table it yields $\psi(0)<\infty$, and therefore we recover $\langle\Psi(0)\rangle\equiv 0$, that is understandable due to the deterministic nature of the pressure head at the water table. The overall utility of the proposed model is that it enables one to assess, into a simple and quick manner, the impact of the water table upon the nonstationary behavior of the FVs, by providing, in particular, explicit relationships between the input parameters and the model output.

Besides the general relevance, results of the present paper are shown to be useful toward the practical applications. Indeed, the model is tested against a recently conducted flow experiment in the vadose zone [*Comegna et al*., 2010; *Severino et al*., 2010, 2016a]. We use independent (no calibration) univariate analysis to identify the mean, and variance of $Y=\ln K_s$ and $\zeta=\ln\alpha$. In particular, the significantly small ($\sim$2 orders of magnitude) variance of ζ as compared with that of Y authorizes limiting our analysis to the zero-order approximation in σ_ζ, and to the second-order approximation in σ_Y. By using the same data set, we determine the horizontal integral scale I pertaining to Y, whereas to identify the anisotropy ratio λ we have used three batteries of (shallow) steady state measurements of the pressure head Ψ. To check the reliability of the estimated value of λ, we have compared the experimental cross-variance Ψ–Y as determined by independent (i.e., not used for calibration purposes) data against to the theoretical asymptotic cross-variance $\sigma_{\Psi Y}(\infty)$. The very satisfactory comparison (combined with prior geological information) with the measurements corroborates the achieved results.

Once the input soil properties are identified, we have analyzed the flow behavior close to the water table. The listed below major conclusions were achieved:

1. the infiltrating flux q_0 and the integral scale/impact the stationary values of the specific flux $(q_h,q_z)^\top$, whereas they have a limited influence upon the distance from the water table at which such stationary values are attained;
2. from the application point of view, one can estimate the thickness of the flow domain where the nonstationary is dominant by means of a 1-D Richards equation (i.e., valid for the vertical mean pressure head $\langle\Psi\rangle$).

Although we have limited the discussion to the data of the Ponticelli's experiment, the vadose zone flow model derived in the present study is rather general. Thus, one can assess the impact of: (i) the spatial variability of the ζ-parameter, (ii) the cross-correlation Y–ζ that in some circumstances may result relevant [see, e.g., *Russo et al*., 1997], and (iii) the various correlation length scales. These studies are topics of ongoing researches. Finally, we also hope that our results will be beneficial for other theoretical/experimental studies dealing with flow (and transport) under similar conditions.

Appendix A: Derivation of C_{Ψ_γ} and C_Ψ

We preliminarily switch into (27) to the new variable $\boldsymbol{r}_h=\boldsymbol{x}_h-\boldsymbol{x}'_h\equiv(x-x',y-y')\in\mathbb{R}^2$, and subsequently take the (2-D) Fourier transform: $\tilde{f}(\boldsymbol{k})=(2\pi)^{-1}\int d\boldsymbol{r}_h\exp(j\boldsymbol{k}\cdot\boldsymbol{r}_h)f(\boldsymbol{r}_h)$ in the horizontal plane $\boldsymbol{r}_h\in\mathbb{R}^2$, to have:

$$\mathcal{L}_{k^2}\tilde{\Phi}(k,z,z')=-\sqrt{-q_0}\exp\left(\frac{z}{2}\right)\frac{d}{dz}\left[\bar{\sigma}_{Y_\gamma}\tilde{\rho}_h(kI_{Y_\gamma})\rho_v\left(\frac{z-z'}{\bar{\lambda}_{Y_\gamma}}\right)+\bar{\sigma}_{\zeta_\gamma}\Psi_0(z)\tilde{\rho}_h(kI_{\zeta_\gamma})\rho_v\left(\frac{z-z'}{\bar{\lambda}_{\zeta_\gamma}}\right)\right] \quad \text{(A1)}$$

where we have set $\mathcal{L}_\alpha \equiv \frac{d^2}{dz^2} - \left(\alpha + \frac{1}{4}\right)$, $\bar{\sigma}_{\eta\gamma} \equiv \sigma_{\eta\gamma} I_{\eta\gamma}$, and $\bar{\lambda}_{\eta\gamma} \equiv \lambda_{\eta\gamma} I_{\eta\gamma}$ $(\eta = Y, \zeta)$. Thus, in the mixed domain $\{(\boldsymbol{k}, z) : \boldsymbol{k} \in \mathbb{R}^2, z \geq 0\}$ the resulting ODE is solved by the Green function (30), solution of the problem: $\mathcal{L}_{k^2} G_\beta(z, z') = \delta(z - z')$, to end up (after integrating by parts) with

$$\tilde{C}_{\Psi\gamma}(k, z, z') = g(z) \int_0^\infty d\xi \left[\bar{\sigma}_{Y\gamma}\, \tilde{\rho}_h(k I_{Y\gamma})\, \rho_v\left(\frac{\xi - z'}{\bar{\lambda}_{Y\gamma}}\right) + \bar{\sigma}_{\zeta\gamma}\, \Psi_0(\xi)\, \tilde{\rho}_h(k I_{\zeta\gamma})\, \rho_v\left(\frac{\xi - z'}{\bar{\lambda}_{\zeta\gamma}}\right) \right] \frac{d}{d\xi} \left[\exp\left(\frac{\xi}{2}\right) G_\beta(z, \xi) \right]. \tag{A2}$$

In order to calculate the inverse of (A2) we need to evaluate the following integral:

$$\mathcal{I}(r) = \int \frac{d\boldsymbol{k}}{2\pi} \exp(-j\boldsymbol{k} \cdot \boldsymbol{r}) \tau(k), \tag{A3}$$

being τ any integrable function depending only upon the modulus of the wave number $\boldsymbol{k}$. Thus, we first adopt polar coordinates: $k(\cos\theta, \sin\theta)$, and subsequently choose the polar axis $\boldsymbol{k}$ in the direction of $\boldsymbol{r}$, so that $\boldsymbol{k} \cdot \boldsymbol{r} = k r \cos\theta$. By noting that $\int_0^{2\pi} d\theta \exp(-j k r_h \cos\theta) = 2\pi J_0(k r)$, (A3) writes as $\mathcal{I}(r) = \int_0^\infty dk\, k\, J_0(k r)\, \tau(k)$. This together with (A2) leads to (28).

To compute the head-covariance C_Ψ, we proceed into a similar manner. Thus, we first apply the transformation (26) (with $C_{\Psi\gamma}$ replaced by C_Ψ) to convert (31) into the following:

$$\nabla^2 \Phi(\boldsymbol{x}, \boldsymbol{x}') - \frac{1}{4} \Phi(\boldsymbol{x}, \boldsymbol{x}') = -\sqrt{-q_0} \exp\left(\frac{z}{2}\right) \frac{\partial}{\partial z} [C_{\Psi Y}(\boldsymbol{x}', \boldsymbol{x}) + \langle \Psi(z) \rangle C_{\Psi\zeta}(\boldsymbol{x}', \boldsymbol{x})]. \tag{A4}$$

Then, we apply the 2-D Fourier transform to (A4) and solve for the Fourier transform of the function Φ (we omit the straightforward derivations). Hence, the Fourier transform $\tilde{C}_\Psi(k, z, z') = \sqrt{-q_0}\, \frac{\exp(-z/2)}{K_r[\Psi_0(z)]}\, \tilde{\Phi}(k, z, z')$ of the head-covariance reads as

$$\tilde{C}_\Psi(k, z, z') = g(z) \int_0^\infty d\xi \left[\tilde{C}_{\Psi Y}(k, z', \xi) + \Psi_0(\xi) \tilde{C}_{\Psi\zeta}(k, z', \xi) \right] \frac{d}{d\xi} \left[\exp\left(\frac{\xi}{2}\right) G_\beta(z, \xi) \right]. \tag{A5}$$

Substitution of (A2), and taking the inverse Fourier-transform of (A5), leads to (32).

Appendix B: Computation of the Variance $\sigma^2_{q_z}$ of the Vertical Flux

To this aim, we preliminary observe that

$$\frac{\partial}{\partial \zeta} \mathcal{G}_\beta(z, \zeta)|_{\zeta \equiv z} = \frac{1}{4}(2\beta - 1)\exp(-z\beta) - \frac{\exp(z)}{4\beta} \left[\beta^2 + 6\beta - 2 + (\beta^2 - 3\beta + 2)\exp(-z\beta)\right] \tag{B1}$$

$$\begin{aligned} \frac{\partial^2}{\partial z \partial \zeta} \mathcal{G}_\beta(z, \zeta)|_{\zeta \equiv z} &= \frac{1}{8}(\beta^3 - 2\beta^2 + 2\beta - 2)\exp(-z\beta) + \\ &- \frac{\exp(z)}{8\beta} \left[\beta^4 + 2\beta^3 + 4\beta^2 + 4\beta - 2 - 2(2\beta^3 - 2\beta^2 + 4\beta - 1)\exp(-z\beta)\right]. \end{aligned} \tag{B2}$$

The derivatives (B1)–(B2) have been obtained (we omit the very lengthy algebraic derivations) by: (i) differentiating (52), (ii) accounting for (54), and (iii) making use of the straightforward identities

$$-\frac{\partial}{\partial z} G_\beta(z, \xi) = \frac{\partial}{\partial \xi} G_\beta(z, \xi) + \exp\left[-\frac{1}{2}(z + \xi)\beta\right], \tag{B3}$$

$$-\frac{\partial^2}{\partial z \partial \xi} G_\beta(z, \xi) = \frac{\beta^2}{4} G_\beta(z, \xi) + \delta(\xi - z) - \frac{\beta}{2} \exp\left[-\frac{1}{2}(z + \xi)\beta\right]. \tag{B4}$$

By recalling that: (i) $\Upsilon(z, \zeta) \equiv \int_0^\infty dk\, k\, \rho_h(k)\, \mathcal{G}_\beta(z, \zeta)$, (ii) $\frac{\partial}{\partial \zeta} \Upsilon(z, \zeta) \equiv \int_0^\infty dk\, k\, \rho_h(k)\, \frac{\partial}{\partial \zeta} \mathcal{G}_\beta(z, \zeta)$ and (iii) $\frac{\partial^2}{\partial z \partial \zeta} \Upsilon(z, \zeta) \equiv \int_0^\infty dk\, k\, \rho_h(k)\, \frac{\partial^2}{\partial z \partial \zeta} \mathcal{G}_\beta(z, \zeta)$, one ends up (after taking the limit $\zeta \to z$, and carrying out the quadrature over k) with

$$\Upsilon(z, \zeta)|_{\zeta \equiv z} = -\frac{1}{2}\exp(z)\Upsilon_1(z), \quad \frac{\partial}{\partial \zeta} \Upsilon(z, \zeta)|_{\zeta \equiv z} = -\frac{1}{4}\exp(z)\Upsilon_2(z), \quad \frac{\partial^2}{\partial z \partial \zeta} \Upsilon(z, \zeta)|_{\zeta \equiv z} = -\frac{1}{8}\exp(z)\Upsilon_3(z) \tag{B5}$$

$$\Upsilon_1(z)=\pi(2\pi z^2-2z+1)\Lambda(2z)-\pi\Lambda(0)+2\exp(-z)-(2\pi z-1)\exp(-2z)-3, \quad \text{(B6)}$$

$$\Upsilon_2(z)=(\pi-1)\Lambda(0)-(2\pi^2z^2-2\pi z+\pi-1)\Lambda(2z)+(4\pi z-1)\exp(-2z)-2(\pi z+1)\exp(-z)+7, \quad \text{(B7)}$$

$$\Upsilon_3(z)=(6\pi^2+4\pi-1)\Lambda(0)-[8\pi^4z^4-8\pi^3z^3+4\pi^2(6\pi-1)z^2-6\pi(2\pi+1)z+6\pi^2-2\pi-1]\Lambda(2z)+ \\ +[8\pi^3z^3+4\pi^2z^2+2\pi(10\pi+1)z+2\pi+1]\exp(-2z)-8(2\pi^2z^2+2\pi+1)\exp(-z)+14\pi+11. \quad \text{(B8)}$$

Acknowledgments
The first author acknowledges support from: (i) "Programma di scambi internazionali per mobilita' di breve durata" (Naples University, Italy), and (ii) "OECD Cooperative Research Programme: Biological Resource Management for Sustainable Agricultural Systems" (contract JA00073336). The constructive comments from the three anonymous Referees and Xavier Sanchez-Vila were deeply appreciated. All data can be found in the supporting information.

References

Andersson, J., and A. Shapiro (1983), Stochastic analysis of one-dimensional steady state unsaturated flow: A comparison of Monte Carlo and perturbation methods, *Water Resour. Res.*, *19*(1), 121–133.
Barajas-Solano, D. A., and D. M. Tartakovsky (2016), Stochastic collocation methods for nonlinear parabolic equations with random coefficients, *SIAM/ASA J. Uncert. Quant.*, *4*(1), 475–494, doi:10.1137/130930108.
Basile, A., G. Ciollaro, and A. Coppola (2003), Hysteresis in soil water characteristics as a key to interpreting comparisons of laboratory and field measured hydraulic properties, *Water Resour. Res.*, *39*(12), 1355, doi:10.1029/2003WR002432.
Brooks, P. M., and A. T. Corey (1964), *Hydraulic Properties of Porous Media, Hydrol. Pap. 3*, Colorado State University, Fort Collins, Colo.
Comegna, A., G. Severino, and A. Sommella (2006), Surface measurements of hydraulic properties in an irrigated soil using a disc permeameter, *WIT Trans. Ecol. Environ*, *96*, 341–353.
Comegna, A., A. Coppola, V. Comegna, G. Severino, A. Sommella, and C. Vitale (2010), State-space approach to evaluate spatial variability of field measured soil water status along a line transect in a volcanic-vesuvian soil, *Hydrol. Earth Syst. Sci.*, *14*(12), 2455–2463.
Comegna, A., A. Coppola, G. Dragonetti, G. Severino, A. Sommella, and A. Basile (2013), Dielectric properties of a tilled sandy volcanic-vesuvian soil with moderate andic features, *Soil Tillage Res.*, *133*, 93–100.
Comegna, V., and A. Basile (1994), Temporal stability of spatial patterns of soil water storage in a cultivated vesuvian soil, *Geoderma*, *62*(1–3), 299–310.
Comegna, V., P. Damiani, F. D'Anna, and C. Ruggiero (1996), Comparison of different field methods for determining the hydraulic conductivity curve of a volcanic vesuvian soil, *Geoderma*, *73*(3–4), 231–244.
Fallico, C., S. De Bartolo, M. Veltri, and G. Severino (2016), On the dependence of the saturated hydraulic conductivity upon the effective porosity through a power law model at different scales, *Hydrol. Processes*, *30*(13), 2366–2372, doi:10.1002/hyp.10798.
Ferrante, M., and T.-C. J. Yeh (1999), Head and flux variability in heterogeneous unsaturated soils under transient flow conditions, *Water Resour. Res.*, *35*(5), 1471–1479.
Fiori, A., P. Indelman, and G. Dagan (1998), Correlation structure of flow variables for steady flow toward a well with application to highly anisotropic heterogeneous formations, *Water Resour. Res.*, *34*(4), 699–708, doi:10.1029/97WR02491.
Fiori, A., F. Boso, F. P. de Barros, S. De Bartolo, A. Frampton, G. Severino, S. Suweis, and G. Dagan (2010), An indirect assessment on the impact of connectivity of conductivity classes upon longitudinal asymptotic macrodispersivity, *Water Resour. Res.*, *46*, W08601, doi:10.1029/2009WR008590.
Gardner, W. R. (1958), Some steady state solutions of unsaturated moisture flow equations with application to evaporation from a water table, *Soil Sci.*, *85*, 228–232.
Gillham, R. (1984), The capillary fringe and its effect on water-table response, *J. Hydrol.*, *67*(1), 307–324, doi:10.1016/0022-1694(84)90248-8.
Gómez, S., G. Severino, L. Randazzo, G. Toraldo, and J. Otero (2009), Identification of the hydraulic conductivity using a global optimization method, *Agric. Water Manage.*, *96*(3), 504–510.
Hillel, D. (1998), *Environmental Soil Physics*, Academic, San Diego, Calif.
Indelman, P., and G. Dagan (1999), Solute transport in divergent radial flow through heterogeneous porous media, *J. Fluid Mech.*, *384*, 159–182.
Indelman, P., D. Or, and Y. Rubin (1993), Stochastic analysis of unsaturated steady state flow through bounded heterogeneous formations, *Water Resour. Res.*, *29*(4), 1141–1148.
Jankovic, I., A. Fiori, and G. Dagan (2003), Flow and transport in highly heterogeneous formations: 3. Numerical simulations and comparison with theoretical results, *Water Resources Research*, *39*(9), 1270, doi:10.1029/2002WR001721.
Li, B., and T.-C. Yeh (1998), Sensitivity and moment analyses of head in variably saturated regimes, *Adv. Water Resour.*, *21*(6), 477–485, doi: https://doi.org/10.1016/S0309-1708(97)00011-0.
Mualem, Y. (1976), A new model for predicting the hydraulic conductivity of unsaturated porous media, *Water Resour. Res.*, *12*(3), 513–522.
Ragab, R., and J. D. Cooper (1993a), Variability of the unsaturated zone water transport parameters: Implications for hydrological modelling, 1. in-situ measurements, *J. Hydrol.*, *148*, 109–131.
Ragab, R., and J. D. Cooper (1993b), Variability of the unsaturated zone water transport parameters: Implications for hydrological modelling, 2. predicted vs in-situ measurements and evaluation methods, *J. Hydrol.*, *148*, 133–147.
Romano, N., P. Nasta, G. Severino, and J. Hopmans (2011), Using bimodal lognormal functions to describe soil hydraulic properties, *Soil Sci. Soc. Am. J.*, *75*(2), 468–480.
Rubin, Y. (2003), *Applied Stochastic Hydrogeology*, Oxford Univ. Press, Oxford, U. K.
Russo, D. (1993), Stochastic modeling of macrodispersion for solute transport in a heterogeneous unsaturated porous formation, *Water Resour. Res.*, *29*(2), 383–397.
Russo, D. (2003), Upscaled conductivity in gravity-dominated flow through variably saturated heterogeneous formations, *Water Resour. Res.*, *39*(9), 1255, doi:10.1029/2002WR001857.
Russo, D., and M. Bouton (1992), Statistical analysis of spatial variability in unsaturated flow parameters, *Water Resour. Res.*, *28*(7), 1911–1925.
Russo, D., and E. Bresler (1981), Soil hydraulic properties as stochastic processes: I. an analysis of field spatial variability, *Soil Sci. Soc. Am. J.*, *45*(4), 682–687.
Russo, D., and A. Fiori (2008), Equivalent vadose zone steady-state flow. an assessment of its applicability to predict transport in a realistic combined vadose zone-groundwater flow system, *Water Resour. Res.*, *44*, W09436, doi:10.1029/2007WRR006170.
Russo, D., and A. Fiori (2009), Stochastic analysis of transport in a combined heterogeneous vadose zone–groundwater flow system, *Water Resour. Res.*, *45*, W03426, doi:10.1029/2008WR007157.
Russo, D., I. Russo, and A. Laufer (1997), On the spatial variability of parameters of the unsaturated hydraulic conductivity, *Water Resour. Res.*, *33*(5), 947–956.

Russo, D., A. Laufer, A. Silber, and S. Assouline (2009), Water uptake, active root volume and solute leaching under drip irrigation: A numerical study, *Water Resources Research*, *45*, W12413, doi:10.1029/2008WR008015.
Severino, G. (2011a), Stochastic analysis of well-type flows in randomly heterogeneous porous formations, *Water Resour. Res.*, *47*, W03520, doi:10.1029/2010WR009840.
Severino, G. (2011b), Macrodispersion by point-like source flows in randomly heterogeneous porous media, *Transp. Porous Media*, *89*(1), 121–134.
Severino, G., and S. D. Bartolo (2015), Stochastic analysis of steady seepage underneath a water-retaining wall through highly anisotropic porous media, *J. Fluid Mech.*, *778*, 253–272.
Severino, G., and A. Coppola (2012), A note on the apparent conductivity of stratified porous media in unsaturated steady flow above a water table, *Transp. Porous Media*, *91*(2), 733–740, doi:10.1007/s11242-011-9870-2.
Severino, G., and P. Indelman (2004), Analytical solutions for reactive transport under an infiltration–redistribution cycle, *J. Contam. Hydrol.*, *70*(1), 89–115.
Severino, G., and A. Santini (2005), On the effective hydraulic conductivity in mean vertical unsaturated steady flows, *Adv. Water Resour.*, *28*, 964–974.
Severino, G., and D. M. Tartakovsky (2015), A boundary-layer solution for flow at the soil-root interface, *J. Math. Biol.*, *70*(7), 1645–1668, doi:10.1007/s00285-014-0813-8.
Severino, G., A. Santini, and A. Sommella (2003), Determining the soil hydraulic conductivity by means of a field scale internal drainage, *J. Hydrol.*, *273*(1–4), 234–248.
Severino, G., V. Monetti, A. Santini, and G. Toraldo (2006), Unsaturated transport with linear kinetic sorption under unsteady vertical flow, *Transp. Porous Media*, *63*(1), 147–174.
Severino, G., V. Cvetkovic, and A. Coppola (2007), Spatial moments for colloid-enhanced radionuclide transport in heterogeneous aquifers, *Adv. Water Resour.*, *30*(1), 101–112.
Severino, G., A. Santini, and V. M. Monetti (2009), Modelling water flow and solute transport in heterogeneous porous media, in *Advances in Modeling Agricultural Systems*, edited by P. J. Papajorgji and P. M. Pardalos, pp. 361–383, Springer, New York.
Severino, G., A. Comegna, A. Coppola, A. Sommella, and A. Santini (2010), Stochastic analysis of a field-scale unsaturated transport experiment, *Adv. Water Resour.*, *33*(10), 1188–1198, doi:10.1016/j.advwatres.2010.09.004.
Severino, G., D. Tartakovsky, G. Srinivasan, and H. Viswanathan (2012a), Lagrangian models of reactive transport in heterogeneous porous media with uncertain properties, *Proc. R. Soc. A*, *468*(2140), 1154–1174.
Severino, G., S. De Bartolo, G. Toraldo, G. Srinivasan, and H. Viswanathan (2012b), Travel time approach to kinetically sorbing solute by diverging radial flows through heterogeneous porous formations, *Water Resour. Res.*, *48*, W12527, doi:10.1029/2012WR012608.
Severino, G., M. Scarfato, and G. Toraldo (2016a), Mining geostatistics to quantify the spatial variability of certain soil flow properties, *Proc. Comput. Sci.*, *98*, 419–424.
Severino, G., G. Toraldo, and D. M. Tartakovsky (2016b), The frequency domain approach to analyse field-scale miscible flow transport experiments in the soils, *Biosyst. Eng.*, doi:10.1016/j.biosystemseng.2016.10.002, in press.
Sinsbeck, M., and D. M. Tartakovsky (2015), Impact of data assimilation on cost-accuracy tradeoff in multifidelity models, *SIAM/ASA J. Uncert. Quant.*, *3*(1), 954–968, doi:10.1137/141001743.
Tartakovsky, A. M., L. Garcia-Naranjo, and D. M. Tartakovsky (2004), Transient flow in a heterogeneous vadose zone with uncertain parameters, *Vadose Zone J.*, *3*(1), 154–163.
Tartakovsky, D. M., S. P. Neuman, and Z. Lu (1999), Conditional stochastic averaging of steady state unsaturated flow by means of Kirchhoff transformation, *Water Resour. Res.*, *35*(3), 731–745.
Tartakovsky, D. M., A. Guadagnini, and M. Riva (2003), Stochastic averaging of nonlinear flows in heterogeneous porous media, *J. Fluid Mech.*, *492*, 47–62, doi:10.1017/S002211200300538X.
Terribile, F., A. Basile, R. De Mascellis, M. Iamarino, P. Magliulo, S. Pepe, and S. Vingiani (2007), Landslide processes and andosols: The case study of the Campania region, Italy, in *Soils of Volcanic Regions in Europe: Volcanic Soils and Land Use*, edited by Ó. Arnalds et al., 545–563, Springer, Berlin, Heidelberg, New York.
Van Genuchten, M. T. (1980), Some steady state solutions of unsaturated moisture flow equations with application to evaporation from a water table, *Soil Sci. Soc. Am. J.*, *44*, 892–898.
Wang, P., P. Quinlan, and D. M. Tartakovsky (2009), Effects of spatiotemporal variability of precipitation on contaminant migration in vadose zone, *Geophys. Res. Lett.*, *36*, L12404, doi:10.1029/2009GL038347.
White, I., and M. Sully (1992), On the variability and use of the hydraulic conductivity alpha parameter in stochastic treatment of unsaturated flow, *Water Resour. Res.*, *28*(1), 209–213.
Wierenga, P., R. Hills, and D. Hudson (1991), The las cruces trench site: Characterization, experimental results, and one-dimensional flow predictions, *Water Resour. Res.*, *27*(10), 2695–2705.
Yeh, T.-C. J., Gelhar, W. L., and G. A. (1985), Stochastic analysis of unsaturated flow in heterogenous soils, 1. Statistically isotropic media, *Water Resour. Res.*, *21*(4), 447–456.
Zhang, D. (2002), *Stochastic Methods for Flow in Porous Media*, Academic, San Diego, Calif.
Zhang, D., and C. L. Winter (1998), Nonstationary stochastic analysis of steady state flow through variably saturated, heterogeneous media, *Water Resour. Res.*, *34*(5), 1091–1100.